Glycogen Synthase Kinase 3 regulates the genesis of displaced retinal ganglion cells

Elena Kisseleff, Robin J Vigouroux, Catherine Hottin, Sophie Lourdel, Leah Thomas, Parth Shah, Alain Chédotal, Muriel Perron, Anand Swaroop, Jérôme E. Roger

▶ To cite this version:

Elena Kisseleff, Robin J Vigouroux, Catherine Hottin, Sophie Lourdel, Leah Thomas, et al.. Glycogen Synthase Kinase 3 regulates the genesis of displaced retinal ganglion cells. eNeuro, 2021, 8 (3), pp.ENEURO.0171-21.2021. 10.1523/ENEURO.0171-21.2021 . hal-03354295

HAL Id: hal-03354295

https://hal.sorbonne-universite.fr/hal-03354295

Submitted on 24 Sep 2021

HAL is a multi-disciplinary open access archive for the deposit and dissemination of scientific research documents, whether they are published or not. The documents may come from teaching and research institutions in France or abroad, or from public or private research centers.

L'archive ouverte pluridisciplinaire **HAL**, est destinée au dépôt et à la diffusion de documents scientifiques de niveau recherche, publiés ou non, émanant des établissements d'enseignement et de recherche français ou étrangers, des laboratoires publics ou privés.

eNeuro

Research Article: New Research | Sensory and Motor Systems

Glycogen Synthase Kinase 3 regulates the genesis of displaced retinal ganglion cells

https://doi.org/10.1523/ENEURO.0171-21.2021

Cite as: eNeuro 2021; 10.1523/ENEURO.0171-21.2021

Received: 19 April 2021
Revised: 19 August 2021
Accepted: 2 September 2021

This Early Release article has been peer-reviewed and accepted, but has not been through the composition and copyediting processes. The final version may differ slightly in style or formatting and will contain links to any extended data.

Alerts: Sign up at www.eneuro.org/alerts to receive customized email alerts when the fully formatted version of this article is published.

Copyright © 2021 Kisseleff et al.
This is an open-access article distributed under the terms of the Creative Commons Attribution 4.0 International license, which permits unrestricted use, distribution and reproduction in any medium provided that the original work is properly attributed.

eNeuro Accepted Manuscript

eNeuro Accepted Manuscript

Glycogen Synthase Kinase 3 regulates the genesis of displaced retinal ganglion cells.

Elena Kisseleff[1], Robin J Vigouroux[3], Catherine Hottin[1], Sophie Lourdel[1], Leah Thomas[1], Parth Shah[2], Alain Chédotal[3], Muriel Perron[1]*, Anand Swaroop[2]* and Jerome E Roger[1,2]*

[1] Paris-Saclay Institute of Neuroscience, CERTO-Retina France, CNRS, Université Paris-Saclay, Orsay 91405, France

[2] Neurobiology-Neurodegeneration and Repair Laboratory, National Eye Institute, National Institutes of Health, Bethesda, MD, USA

[3] Sorbonne Universités, UPMC Université Paris 06, INSERM, CNRS, Institut de la Vision, 75012 Paris, France

Running Title: **GSK3 controls displaced retinal ganglion cell genesis in the retina**

*Corresponding authors:

- Jerome E Roger. jerome.roger@universite-paris-saclay.fr
- Anand Swaroop. swaroopa@nei.nih.gov
- Muriel Perron. muriel.perron@universite-paris-saclay.fr

eNeuro Accepted Manuscript

26

27 ## ABSTRACT

28 Glycogen Synthase Kinase 3 (GSK) proteins (GSK3α and GSK3β) are key mediators
29 of signaling pathways, with crucial roles in coordinating fundamental biological
30 processes during neural development. Here we show that the complete loss of GSK3
31 signaling in mouse retinal progenitors leads to microphthalmia with broad
32 morphological defects. A single wild-type allele of either *Gsk3α* or *Gsk3β* is able to
33 rescue this phenotype. In this genetic context, all cell types are present with a
34 functional retina. However, we unexpectedly detect a large number of cells in the
35 inner nuclear layer expressing retinal ganglion cell (RGC)-specific markers (called
36 displaced RGCs, dRGCs) when at least one allele of *Gsk3α* is expressed. Excess
37 dRGCs lead to increased number of axons projecting into the ipsilateral medial
38 terminal nucleus, an area of the brain belonging to the non-image-forming visual
39 circuit and poorly targeted by RGCs in wild-type retina. Transcriptome analysis and
40 optomotor response assay suggest that at least a subset of dRGCs in *Gsk3* mutant
41 mice are direction-selective RGCs. Our study thus uncovers a unique role of GSK3 in
42 controlling the production of ganglion cells in the inner nuclear layer, which
43 correspond to dRGCs, a rare and poorly characterized retinal cell type.

44

45

eNeuro Accepted Manuscript

46
Significance Statement

47 Glycogen Synthase Kinase 3 (GSK) proteins (Gsk3α or Gsk3β) are key mediators of
48 signaling pathways, especially in the central nervous system but poorly described in
49 the retina. Here we show that the complete loss of GSK3 in mouse retinal progenitors
50 leads to microphthalmia. However, when only one allele of *Gsk3α* or *Gsk3β* are
51 present, all cell types are present with a functional retina. More importantly, we
52 unexpectedly uncover a unique role of GSK3 in controlling the genesis of retinal
53 ganglion cells in the inner nuclear layer which could correspond to a rare and poorly
54 characterized retinal cell type. Therefore, our mouse models potentially offer a unique
55 and powerful model system to study the visual function of dRGCs in mammals.
56
57

58 ## INTRODUCTION

59 Glycogen Synthase Kinase 3 alpha (GSK3α) and beta (GSK3β) are
60 functionally redundant serine/threonine kinases encoded by two different genes,
61 sharing 95% identity in their kinase domain (Doble et al., 2007). GSK3 exists at the
62 crossroads of multiple signaling pathways and acts as a key molecular switch to
63 mediate their output and guide distinct cellular processes (Cole, 2012; Doble and
64 Woodgett, 2003; Espinosa et al., 2003; Jin et al., 2009; Shimizu et al., 2008; Wang
65 and Li, 2006). Among the signaling pathways regulated by GSK3 kinases, Wnt
66 canonical pathway is the most well described, with GSK3β inhibition triggering an
67 increase in β-catenin protein levels and its nuclear translocation to activate target
68 gene expression (Doble and Woodgett, 2003).

69 GSK3 is a key regulator of neural stem/precursor cell proliferation in
70 developing as well as adult brain (Eom and Jope, 2009; Hur and Zhou, 2010; Kim et
71 al., 2009; Pachenari et al., 2017). Conditional deletion and gain of function
72 experiments indicate that GSK3 promotes neuronal differentiation (Hur and Zhou,
73 2010; Kim et al., 2009). GSK3 exerts its effects through phosphorylation of keys
74 proteins involved in neural development, including proneural factors such as
75 Neurogenin 2 and NeuroD (Li et al., 2012; Moore et al., 2002). In addition, GSK3
76 fine-tunes the balance between cell death and survival, and its altered function is
77 associated with neurodegenerative pathologies including Alzheimer's disease,
78 bipolar disorders, and Parkinson's disease (Golpich et al., 2015; Jacobs et al., 2012;
79 Kremer, 2011; Li et al., 2014; Maurer et al., 2014; Medina et al., 2011).

80 GSK3 kinases are widely expressed in the developing retina (Pérezleón et al.,
81 2013). GSK3-dependent phosphorylation is shown to control the timing of proneural
82 factor activity and thereby regulate retinal cell fate determination. For instance,
83 inhibition of GSK3 signaling in the developing *Xenopus* retina leads to increase in

eNeuro Accepted Manuscript

eNeuro Accepted Manuscript

84 early-born cell types at the expense of late-born cells (Marcus et al., 1998; Moore et
85 al., 2002).
86 To elucidate GSK3 function in mammalian retina development, we generated
87 conditional loss-of-function alleles of *Gsk3α* and *Gsk3β* in retinal progenitor cells. We
88 show that complete loss of both GSK3 kinases severely impacts retinal morphology
89 with microphthalmia phenotype, which could be completely rescued with the
90 expression of just one *Gsk3α* or *Gsk3β* wild-type allele. We also noted the presence
91 of a large number of displaced retinal ganglion cells (dRGCs) in the inner nuclear
92 layer in the absence of either *Gsk3α* or *Gsk3β*. In normal conditions, this is a rare
93 retinal cell subtype, poorly characterized so far. Anterograde labeling of the axonal
94 ganglion cell projections into the brain of *Gsk3* mutant mice, allowed us to further
95 support their dRGCs identity. Our study thus identifies GSK3 as a possible
96 determinant of dRGC genesis. We also provide transcriptomic data and visual tests
97 suggesting that at least a subset of these supernumerary dRGCs in *Gsk3* mutant
98 retinas are direction-selective RGCs.
99

100 MATERIALS AND METHODS

101 Animals and tissue collection

102 All animal experiments have been carried out in accordance with the European
103 Communities Council Directive of 22 September 2010 (2010/63/EEC), European
104 Union guidelines effective and with the Association for Research in Vision and
105 Ophthalmology statement for the use of animals in ophthalmic and visual Research.
106 All animal care and experimentation were also conducted in accordance with
107 guidelines, under the license APAFIS#1018-2016072611404304 by the Institutional
108 animal care committee n°059 in France and by Animal Care and Use Committee at

eNeuro Accepted Manuscript

109 the National Institutes of Health (ASP#650). *Gsk3α* and *Gsk3β* floxed mice were
110 generously provided by Dr. Jim Woodgett (University of Toronto, Canada). Floxed
111 *Gsk3* mice were mated with those carrying the retina-specific regulatory element of
112 murine *Pax6* driving the expression of the Cre recombinase (*α-Cre*) in retinal
113 progenitors as early as E10.5 generously provided by Peter Gruss (Roger et al.,
114 2012). Mice are on a mixed background C57Bl6/J and 129/SvJ. Animals from either
115 sex were used for experimental procedures. All mouse genotyping was performed as
116 described (Hamon et al., 2019).

117 **Hematoxylin & eosin (H&E) staining, and immunostaining**

118 Methacrylate sections were used for H&E staining as previously described (Hamon et
119 al., 2019). For IHC on frozen sections, enucleated eyeballs were fixed at the required
120 stage in 4% PFA for 60 min on ice and incubated in an increasing concentration of
121 sucrose (10%, 20% and 30%), then embedded in OCT. Embedded eyeballs were
122 serially cut to 12 µm sections using a cryostat. For embryonic stages, pregnant
123 females were euthanized and whole heads of pups were harvested in paraffin. IHC
124 was performed as described (Kretschmer et al., 2015, 2013). Primary and secondary
125 antibodies are listed in Table 1. Sections were counterstained with 1:1000 4′,6-
126 diamidino-2-phenylindole (DAPI) (1 mg/mL, Thermo Scientific).

127 **EdU labeling and TUNEL assay**

128 For EdU labelling, females were injected intraperitoneally with 10 mM of 5-ethynyl-
129 20-deoxyuridine (EdU) (Life Technology). EdU incorporation was detected on paraffin
130 sections or frozen sections using the Click-iT EdU Imaging Kit following
131 manufacturer’s recommendations (Life Technology). Apoptosis was detected by
132 terminal deoxynucleotidyl transferase-mediated biotinylated UTP nick end labeling
133 (TUNEL) assays using *in situ* cell death detection kit (Promega). All images were
134 acquired using a Zeiss LSM710 confocal microscope and Zen software (Zeiss).

eNeuro Accepted Manuscript

135 **Immunoblotting**

136 Frozen retinas were lysed by sonication in lysis buffer (20 mM Na_2HPO4, 250 mM
137 NaCl, 30 mM NaPPi, 0.1% NP40, 5mM EDTA, 5mM DTT) supplemented with
138 protease inhibitor cocktail (Sigma-Aldrich). Lysates concentration was determined
139 using a Lowry protein assay kit (Bio-Rad) following sonication and centrifugation.
140 Protein supernatants were separated under denaturing condition by SDS-PAGE,
141 transferred onto nitrocellulose membrane and probed with antibodies (listed in Table
142 1), as described (Belle et al., 2017, 2014). Proteins were visualized using enhanced
143 chemiluminescence kit (Bio-Rad). α-tubulin was used for normalization.
144 Quantification was performed using ImageJ software (http://imagej.nih.gov/ij/;
145 provided in the public domain at NIH).

146 **Retinal flat mount**

147 Fixed retinas were permeabilized and blocked in a solution containing 0.5% Triton-
148 X100, 5% donkey normal serum, 1XPBS, 0.1 g/L thimerosal for 1 day at RT under
149 agitation. Primary antibodies were diluted in a solution containing 0.5% Triton-X100,
150 5% donkey normal serum, 10% Dimethyl Sulfoxide, 1XPBS, 0.1 g/L thimerosal for 3
151 days at RT under agitation. The retinas were then washed for 1 day in PBST
152 (1XPBS, 0.5% Triton-X100). Secondary antibodies were diluted in the same solution
153 as primary antibodies and left for 2 days. After washing retinas for 1 day, they were
154 mounted on slides and imaged using a scanning confocal microscope (Olympus,
155 FV1000). Primary and secondary antibodies are listed in Table 1.

156 **Electroretinography**

157 Electroretinogram (ERG) recordings were performed using a focal ERG module
158 attached to Micron IV (Phoenix Research Laboratory). Briefly, mice were dark-
159 adapted overnight and prepared for the experiment under dim-red light. The mice
160 were anesthetized with ketamine (100 mg/kg) and xylazine (10mg/kg) and received

topical proparacaine hydrochloride (0.5%, Alcon) via eye drops. Pupils were dilated with tropicamide (1%, Alcon) and phenylephrine (2.5%, Alcon) and lightly coated with GONAK hypromellose ophthalmic demulcent solution (2.5%, Akorn). Lens of the Micron IV was placed directly on the cornea, and a reference electrode was placed on the mouse head. Scotopic responses were elicited with a series of flashes of increasing light intensities from -1.7 to 2.2 cd.s/m^2. Photopic responses were elicited under rod-desensitizing background light with a series of flashes of increasing light intensities from -0.5 to 2.8 cd.s/m^2. Values of a- and b-wave were extracted and plotted for comparisons between groups of interest.

Optomotor response (OMR)

Real time video tracking and automated measurements of compensatory head movements in freely moving mice were performed using an OMR recording setup (Dobin et al., 2013) (Phenosys, Berlin, Germany). Each mouse was placed on a platform in the center of four computer-controlled LCD monitors. Visual stimuli were sinusoidally modulated luminance gratings generated by four LCD screens (60 Hz refresh rate; OkrArena, PhenoSys GmbH, Berlin, Germany), presented with a constant rotation. Video tracking considered the animal's distance to the monitors, thereby keeping the spatial frequency of the retinal image constant and providing data for automated OMR quantifications.

OMRs were recorded using two different Michelson contrasts and different spatial frequencies (presented in random order) in the two mouse groups: 100% contrast or 50% contrast (n=13 for *Gsk3α$^{f/+}$β$^{f/f}$* and 18 for *Gsk3α$^{f/+}$β$^{f/f}$;α-Cre* genotype). All stimuli were presented for 60 s randomly in either clockwise or counterclockwise direction. The measurements were completed in three trials for each animal. At 100% and 50% contrast, OMRs were recorded in response to sinusoidal gratings at 12 spatial frequencies between 0.0125 and 0.5 cycles per degree (cpd). The number of head

eNeuro Accepted Manuscript

187 movements recorded at a speed range from 2 to 14 degrees per second in the same
188 direction as the stimulus (T_Correct) and in the opposite direction (T_Incorrect) were
189 used to calculate the OMR indices (T_Correct / T_Incorrect) at each spatial
190 frequency.

191 **Retrograde labeling of retinal ganglion cells**

192 For retrograde labeling, eyes were enucleated with a piece of the optic nerve and
193 fixed in 4% PFA for 30 min. Rhodamine B isothiocyanate–Dextran (Sigma-Aldrich)
194 was applied on the top of the optic nerve and incubated for 60 min. Eyes were flat
195 mounted after the remaining dye was washed out for 48 hours in PBS at 4°C. Z
196 series images were acquired using SP5 confocal microscope (Leica Biosystems),
197 and 3D reconstruction was performed using Volocity (Perkin Elmer).

198 **Anterograde labeling of retinal ganglion cell projections**

199 *Anterograde labeling*

200 For anterograde tracing of retinal projections, a Cholera Toxin beta subunit (CTB)
201 was used. Animal were anesthetized using a cocktail of ketamine (60 mg/kg) and
202 xylazine (10 mg/kg) and a subsequent bilateral injection of 1.2uL CTB at 1mg/ml
203 coupled to either an Alexa-555 or -647 (Lifesciences) were performed intravitreally.
204 Three days following the injection, mice were perfused with 4% PFA.

205 *Tissue Clearing and 3D imaging*

206 For 3D imaging of CTB-labeled brains, a methanol clearing protocol was carried out
207 using modification from the iDISCO+ protocol (Dobin et al., 2013). Briefly, brains
208 were dehydrated by immersion in progressive baths of methanol/1X PBS (20%, 40%,
209 60%, 80%, 100%, 100%) for 2 hours each at RT on a tube rotator (SB3, Stuart) at
210 14rpm, using a 15 mL centrifuge tube (TPP, Dutcher) protected from light. Following
211 these baths, samples were immersed overnight in 2/3 Dichloromethane (DCM;

eNeuro Accepted Manuscript

212 Sigma-Aldrich) and then a 30-min bath in 100 % DCM before being transferred in Di-
213 Benzyl Ether (DBE; Sigma-Aldrich) overnight prior imaging.
214 3D imaging/Image acquisition for all samples was performed as previously described
215 (Liao et al., 2014). Acquisitions were done using an ultramicroscope I (LaVision
216 Biotec) with the ImspectorPro software (LaVision Biotec). The step size between
217 each image was fixed at 2 µm with a numerical aperture of 0.120 and 150ms
218 acquisition using a PCO Edge SCMOS CCD camera (2,560 x 2,160 pixel size,
219 LaVision BioTec).
220 *Image analysis*
221 Imaris x64 software (Version9.1.2, Bitplane) was used for all image analysis. Stack
222 images were first converted from .tiff to .ims files using the Imaris file converter
223 v9.1.2. 3D reconstruction was visualized with the “volume rendering” function. To
224 isolate ipsi- and contralateral MTN volumes, manual segmentation was carried out
225 using the “surface” tool and the isoline selection (density, 10%). Each ipsi- and
226 contra-lateral projection of the MTN was segmented to generate a volume (μm^3).
227 Movie reconstruction with .tiff series were done with ImageJ (1.50e, Java 1.8.0_60,
228 64-bit) and iMovie (version 10.1.1).

229 **Whole transcriptome sequencing and data analysis**

230 Whole transcriptome analysis was performed on three independent biological
231 replicates from *Gsk3*$\alpha^{f/+}\beta^{f/f}$*;*α*-Cre* and *Gsk3*$\alpha^{f/+}\beta^{f/f}$ retina at P60. After harvesting, both
232 retinas for each animal were immediately frozen. RNA was extracted using
233 Nucleospin RNA Plus kit (Macherey-Nagel). RNA quality and quantity were evaluated
234 using a BioAnalyzer 2100 with RNA 6000 Nano Kit (Agilent Technologies). Stranded
235 RNA-Seq libraries were constructed from 100 ng high-quality total RNA (RIN > 8)
236 using the TruSeq Stranded mRNA Library Preparation Kit (Illumina). Paired-end
237 sequencing of 40 bases length was performed on a NextSeq 500 system (Illumina).

eNeuro Accepted Manuscript

238 Pass-filtered reads were mapped using STAR and aligned to mouse reference
239 genome GRCm38.94 (Chen et al., 2015). Count table of the gene features was
240 obtained using FeatureCounts (Zhou et al., 2019). Normalization, differential
241 expression analysis and FPKM (fragments per kilobase of exon per million fragments
242 mapped) values were computed using EdgeR (Walter et al., 2015). An FPKM filtering
243 cutoff of 1 in at least one of the 6 samples was applied. A False Discovery Rate
244 (FDR) of less than or equal to 0.05 was considered significant and a fold change
245 cutoff of 1.5 was applied to identify differentially expressed genes. Comprehensive
246 gene list analysis, enriched biological pathways, gene annotation, were based on
247 Gene Ontology classification system using Metascape (Sajgo et al., 2017). Data
248 visualization was done using GOplot R package (Livak and Schmittgen, 2001). To
249 evaluate the expression of the DEGs in RGCs, we used published whole
250 transcriptome analysis from purified RGCs available on Gene Expression Omnibus
251 database (GSE87647) (Livak and Schmittgen, 2001).

252 **Gene expression analysis by Real-Time PCR (RT-qPCR)**

253 After RNA extraction using Nucleospin RNA Plus kit (Macherey-Nagel), 500 ng of
254 total RNA was reverse transcribed using the iScript cDNA Synthesis Kit according to
255 manufacturer instructions (BioRad). Primers used for RT-qPCR are shown in Table 2.
256 For each RT-qPCR, 2 μL of a ten-fold dilution of synthetized cDNA was used, and
257 the reactions were performed in technical triplicates on a C1000 thermal cycler
258 (CFX96 real-time system, BioRad) using SsoFast EvaGreen Supermix (BioRad) as
259 previously described (Livak and Schmittgen, 2001). RT-qPCR experiments were
260 performed on three independent biological replicates. Differential expression was
261 determined using the ΔΔCt method with the geometric average of *Rps26* and *Srp72*
262 as endogenous controls (Livak and Schmittgen, 2001).

eNeuro Accepted Manuscript

263 **Statistical analysis**

264 Statistical analysis was performed with GraphPad Prism 8.3.0 (GraphPad Software,
265 La Jolla California USA). Results are reported as mean ± SEM. Nonparametric
266 Mann-Whitney U test was used to analyze cell counting and qPCR data. P value ≤
267 0.05 was considered significant. For OMR assay statistical analysis, a Grubbs test
268 was performed at 5% to remove outliers followed by 2-way ANOVA (genotype and
269 spatial frequency) with Bonferroni Post Hoc test. P value ≤ 0.05 was considered
270 significant.

271

272 ## RESULTS

273 **Retinal progenitor-specific deletion of both *Gsk3α* and *Gsk3β* results in**
274 **microphthalmia**

275 We crossed the floxed $Gsk3\alpha^{f/f}\beta^{f/f}$ mice with *α-Cre* (*αPax6-Cre*) line to
276 generate $Gsk3\alpha^{f/f}\beta^{f/f}$;*α-Cre* mice in which *Gsk*3 deletion occurs only in retinal
277 progenitors as early as E10.5 (Marquardt et al., 2001). We first validated our model
278 by assessing the efficacy of *Gsk3α* and *Gsk3β* deletion at E12.5 (Figure 1A).
279 Immunohistochemistry (IHC) using an antibody recognizing both GSK3 proteins
280 showed ubiquitous expression in control retinas (Figure 1A). Both *Gsk3* genes were
281 efficiently deleted in the peripheral retina of $Gsk3\alpha^{f/f}\beta^{f/f}$;*α-Cre* mice, but their
282 expression in the central retina remained preserved consistent with the previously
283 described *α-Cre* expression pattern (Marquardt et al., 2001).

284 Hematoxylin and Eosin (H&E) staining revealed major morphological defects
285 with profound retinal disorganization, including the loss of radial arrangement as well
286 as folds and aggregates of retinal progenitor cells (RPCs), in $Gsk3\alpha^{f/f}\beta^{f/f}$;*α-Cre* retina
287 as early as E12.5 (Figure 1B). In addition, blood was detected inside the retinal

eNeuro Accepted Manuscript

288 neuroblastic layer. Structure of the retina worsened rapidly during development
289 although the central part remained unperturbed, consistent with continued *Gsk3*
290 expression in this region. At and after E14.5, the retina was largely reduced whereas
291 the eye size itself was comparable to littermate controls (Figure 1B). A large quantity
292 of blood accumulated inside the eyeball at P2. Finally, growth of the eyeball was
293 severely reduced leading to microphthalmia in the adult (data not shown).
294

295 **Multiple allelic combinations revealed functional redundancy of *Gsk3α* and**
296 ***Gsk3β* in retinal development**

297 Severe deleterious effect by the loss of both *Gsk3α and Gsk3β* in RPCs in
298 early development precludes the analysis of late retinal histogenesis. To circumvent
299 this, we generated animals with different combinations of *Gsk3* deletion (loss of only
300 one *Gsk3* gene: *Gsk3α$^{f/f}$β$^{+/+}$;α-Cre* or *Gsk3α$^{+/+}$β$^{f/f}$;α-Cre*, or ¾ deletion: *Gsk3α$^{f/f}$β$^{f/+}$;α-*
301 *Cre* or *Gsk3α$^{f/+}$β$^{f/f}$;α-Cre*). Immunoblot analysis using anti-GSK3 antibody
302 (recognizing both proteins) in 2-month-old animals with different combinations of
303 *Gsk3α* and *Gsk3β* floxed alleles demonstrated the efficacy of *Gsk3α* and *Gsk3β*
304 deletion in areas where the Cre recombinase was expressed during early retinal
305 development (all retinal progenitors at the exception of a stripe located in the dorso-
306 central region (Roger et al., 2012)) (Figure 2A). IHC analysis using anti-GSK3β
307 showed ubiquitous expression of *Gsk3β* in adult control retina and its complete loss
308 in *Gsk3α$^{f/+}$β$^{f/f}$;α-Cre* retina (Figure 2B). At 2-month, retinal histology revealed the
309 correct laminated architecture with normal photoreceptors and interneurons when
310 even one allele of *Gsk3α* (Figure 2C, D) or *Gsk3β* (data not shown) was present.
311 Photopic and scotopic electroretinogram (ERG) recordings, corresponding to cone
312 and rod function respectively, did not show any significant difference between

eNeuro Accepted Manuscript

313 *Gsk3*$\alpha^{f/+}\beta^{f/f}$*;α-Cre* and control retina (Figure 2E, 2F). These results were similar in
314 mice carrying any combination of *Gsk3* deletion (data not shown). We therefore
315 conclude that a single allele of wild-type *Gsk3α* or *Gsk3β* is sufficient to rescue
316 obvious structural and functional defects in the complete absence of GSK3 signaling.

317 **Loss of either *Gsk3α* or *Gsk3β* in RPCs leads to increased number of displaced**
318 **retinal ganglion cells**

319 Even though a single allele of either *Gsk3α* or *Gsk3β* permitted normal retinal
320 development (Figure 2), we observed a striking increase in the number of RGCs, as
321 indicated by Brn3a-positive cells, in the inner nuclear layer (INL) of *Gsk3*$\alpha^{f/+}\beta^{f/f}$*;α-Cre*
322 retina compared to controls (Figure 3A). Brn3a-positive cells in the INL have been
323 described as displaced retinal ganglion cells (dRGCs), a rare cell type in the
324 mammalian retina (Galli-Resta and Ensini, 1996; Young, 1984). All Brn3a-positive
325 cells in the INL of *Gsk3*$\alpha^{f/+}\beta^{f/f}$*;α-Cre* retina also expressed NF68 that labels cell
326 bodies and axons of RGCs (Figure 3A). To validate that these Brn3a-positive cells in
327 the INL were indeed RGCs with axonal projections included in the optic nerve, we
328 performed retrograde labeling with Rhodamine-Dextran applied onto the optic nerve
329 of *Gsk3*$\alpha^{f/+}\beta^{f/f}$*;α-Cre* mice. Subsequent 3D reconstructions on flat mount retinas
330 revealed the presence of numerous fluorescent cell bodies located in the INL
331 compared to controls (Figure 3B) demonstrating that axons of dRGCs indeed
332 reached the optic nerve. Thus, Brn3a-positive cells located in the INL of
333 *Gsk3*$\alpha^{f/+}\beta^{f/f}$*;α-Cre* retinas are indeed RGCs.

334 Increased dRGCs were observed in retinas carrying any combination of *Gsk3*
335 deletions tested (*Gsk3*$\alpha^{f/f}\beta^{+/+}$, *Gsk3*$\alpha^{+/+}\beta^{f/f}$, *Gsk3*$\alpha^{f/+}\beta^{f/f}$ or *Gsk3*$\alpha^{f/f}\beta^{f/+}$), with the highest
336 number detected in *Gsk3*$\alpha^{f/+}\beta^{f/f}$*;α-Cre* mice compared to controls (10-fold increase)
337 (Figure 3C). Notably, *Gsk3*$\alpha^{f/+}\beta^{f/+}$*;α-Cre* retina did not display excess of dRGCs (data

eNeuro Accepted Manuscript

338 not shown). Interestingly, increase in dRGCs number is not associated with a
339 significant reduction in the number of RGCs in the GCL, referred to as orthotopic
340 RGCs (oRGCs) (Figure 3C).

341 Due to their low number in control retina (around 2% of RGCs), dRGCs have
342 been poorly characterized with very few markers identified, such as Brn3a (Nadal-
343 NicolÃ¡s et al., 2014; Nadal-Nicolás et al., 2012). Immunostaining on sections and flat
344 mount retinas with additional RGC marker antibodies revealed that dRGCs in
345 *Gsk3α$^{f/+}$β$^{f/f}$;α-Cre* retina were also positive for Rbpms (Rodriguez et al., 2014)
346 confirming their increased number in the INL compared to controls (Figure 3D, E).
347 Similar results were observed with Islet1 labeling (Figure 3-1A) (Bejarano-Escobar et
348 al., 2015). Previous work showed that the number of dRGCs varies by retinal domain
349 (Dräger and Olsen, 1980). Counting of Rbpms- or Brn3a-positive dRGCs on
350 *Gsk3α$^{f/+}$β$^{f/f}$;α-Cre* flat mount retinas did not show any significant differences in their
351 distribution between the dorsal, ventral, nasal and temporal regions (Figure 3-1B).
352 Finally, Brn3a-positive dRGCs did not express markers of other INL neurons such as
353 Choline-Acetyltransferase (CHAT, amacrine cells) or Calbindin (horizontal and
354 amacrin cells) (Figure 3-2). Altogether, our results strongly support the ganglion cell
355 identity of the displaced Brn3a- and RPBMS-positive cells located in the INL of
356 *Gsk3α$^{f/+}$β$^{f/f}$;α-Cre.*

357 To test whether dRGCs in *Gsk3* mutant mice were produced during the same
358 developmental time window as oRGCs, we performed pulse chase experiments by
359 injecting EdU at E12.5, at the peak of RGC birth. Retinal sections from one-month-
360 old animals were then immunolabelled using anti-Brn3a antibody (Figure 4A). In
361 control and *Gsk3α$^{f/+}$β$^{f/f}$;α-Cre* retina, we identified 40-50% of RGCs that were
362 Brn3a/EdU-positive in all layers examined (GCL and INL), indicating that both dRGCs
363 and oRGCs were born around the same time (Figure 4B). We next examined

eNeuro Accepted Manuscript

364 whether dRGCs are usually overproduced during normal retinal development and
365 eliminated later on. In this context, increased number of dRGCs in *Gsk3α*$^{f/+}$*β*$^{f/f}$;*α-Cre*
366 retinas could result from a defect in dRGC riddance occurring during the first two
367 postnatal weeks, a period of developmental cell death in the retina (Young, 1984). At
368 P0, the number of Brn3a-positive oRGCs was similar between littermate control and
369 *Gsk3α*$^{f/+}$*β*$^{f/f}$;*α-Cre* retina (Figure 4C and D). In contrast, the proportion of Brn3a-
370 positive cells located in the inner part of neuroblastic layer corresponding presumably
371 to dRGCs was much lower in control retinas (6±0.1%) compared to *Gsk3α*$^{f/+}$*β*$^{f/f}$;*α-Cre*
372 retinas (30±1.4%). Thus, dRGCs are not overproduced and eliminated postnatally in
373 control retina. Our results demonstrate that dRGCs are generated during early waves
374 of retinogenesis in *Gsk3α*$^{f/+}$*β*$^{f/f}$;*α-Cre* retina and strongly suggest that GSK3 kinases
375 play a role in restricting their number during normal retinal development.

376

377 **dRGCs produced in the absence of either *Gsk3α* or *Gsk3β* project to accessory**
378 **visual system circuitry**

379 Previous studies in birds and reptiles have reported that dRGCs could be
380 responsible for optokinetic nystagmus, as they mostly project to the accessory optic
381 nuclei (AOS) (Cook and Podugolnikova, 2001), which is critical for non-image forming
382 circuit and image stabilization (Simpson, 1984). To test whether dRGCs in *Gsk3*
383 mutants project into specific visual nuclei in the brain, including the AOS, we traced
384 the total pool of RGCs, including dRGCs, with Cholera Toxin beta subunit (CTB). Bi-
385 lateral injection of CTB, coupled to either an alexa-555 or -647 followed by 3D
386 imaging, allowed us to trace both ipsi- and contra-lateral projecting axons. We first
387 confirmed that CTB injections indeed marked the dRGCs based on flat mounts of
388 retinas after Brn3a and NF68 immunolabelling (Figure 5-1). To visualize the entire

eNeuro Accepted Manuscript

389 visual projection network, we carried out whole-brain clearing using iDISCO+
390 followed by light-sheet fluorescent imaging and 3D reconstruction (Figure 5A).
391 Complete loss of *Gsk3β* displayed a large increase in ipsilateral projecting RGCs in
392 one of the three nuclei composing the AOS, the Medial Terminal Nucleus (MTN)
393 (Simpson, 1984). This terminal nucleus is the main component of the AOS reacting
394 best to either upward or downward movement and mediates the optokinetic
395 nystagmus critical for image stabilization (Yonehara et al., 2009). Calculation of the
396 signal intensity ratio between the ipsilateral and contralateral MTN demonstrated a
397 significant increase of RGC projections into the ipsilateral MTN in retinas with *Gsk3β*
398 deletion (Figure 5B). This result suggests that excess dRGCs might participate to the
399 non-image forming circuit.

400 **Whole transcriptome analysis suggests that dRGCs in GSK3 mutant retinas are**
401 **direction-selective ganglion cells.**

402 We next performed transcriptome analysis using RNA-sequencing in order to
403 identify molecular changes in adult $Gsk3\alpha^{f/+}\beta^{f/f}$;*α-Cre* retina and to better characterize
404 dRGCs. Retinas from $Gsk3\alpha^{f/+}\beta^{f/f}$ mice were used as controls. Gene level analysis
405 revealed 111 differentially expressed genes (DEGs) using filtering criteria of Fold
406 Change (FC) = 1.5 with a False Discovery rate (FDR) cutoff of ≤ 0.05 and a minimum
407 mean expression value of one FPKM (fragments per kilobase of exon per million
408 reads mapped) in at least one of the two experimental groups (Figure 6A and Figure
409 6-1). Pathway analysis of DEGs revealed several statistically significant
410 overrepresented pathways (Figure 6-2). Biological processes and molecular functions
411 pathways included 48 DEGs; of these, 33 genes were expressed in RGCs based on
412 published whole transcriptomic data from purified RGCs (for a total 69 RGC-
413 expressed genes among the 111 DEGs) (labeled with stars in Figure 8B) (Sajgo et

eNeuro Accepted Manuscript

414 al., 2017). Dominance of RGC-expressed genes in our dataset is consistent with the
415 high number of dRGCs observed in *Gsk3α$^{f/+}$β$^{f/f}$;α-Cre* retina.
416 Among interesting candidates dysregulated in the biological processes and molecular
417 function pathways (Figure 6B and 6-2), we identified *Chrna2*, *Chrna5, Chrna7,*
418 *Chrnb4* encoding for postsynaptic subunits of the nicotinic cholinergic receptor. With
419 the exception of *Chrna2*, all other genes are upregulated in *Gsk3α$^{f/+}$β$^{f/f}$;α-Cre* retina.
420 Most retinal ganglion cells express nicotinic receptors (Kay et al., 2011; Rousso et
421 al., 2016). Among other potentially relevant genes, the *Grik3* gene product belongs to
422 the kainate family of glutamate receptors functioning as ligand-activated ion
423 channels. In direction-selective ganglion cells (DSGCs), glutamate is proposed to be
424 the main source of excitation (Sweeney et al., 2019, 2014). Finally, *Cartpt,* encoding
425 for the preprotein CART (Cocaine- And Amphetamine-Regulated Transcript Protein)
426 that was upregulated in *Gsk3α$^{f/+}$β$^{f/f}$;α-Cre* retina was validated by RT-qPCR (Figure
427 6C). *Cartpt* is specifically expressed in direction-selective RGCs (DS-RGCs) (Rousso
428 et al., 2016; Sato et al., 2017), suggesting that dRGCs (or at least a subset) in
429 *Gsk3α$^{f/+}$β$^{f/f}$;α-Cre* retina might be DS-RGCs. In support with this hypothesis, we found
430 some dRGCs in *Gsk3α$^{f/+}$β$^{f/f}$;α-Cre* and littermate control retina positive for the
431 transcription factor Tbr2, described as essential for RGC specification participating in
432 non-image-forming visual circuits (Figure 6D) (Simpson, 1984; Yonehara et al.,
433 2009). A small subset of dRGCs also expressed Foxp2, a transcription factor
434 involved in DS-RGC differentiation in mice (Figure 6D) (Kim et al., 2009). These two
435 factors were expressed in a mutually exclusive way in Rpbms-positive dRGCs,
436 suggesting that dRGCs in *Gsk3α$^{f/+}$β$^{f/f}$;α-Cre* might encompass several subtypes.
437 **Optomotor response is impaired in GSK3 mutant**
438 Given that DS-RGCs are reported to drive the optomotor response (OMR) by
439 projecting mainly into the contralateral AOS (Kim et al., 2009), we tested the OMR of

eNeuro Accepted Manuscript

440 *Gsk3α*$^{f/+}$*β*$^{f/f}$;*α-Cre* mice. The OMR indices (T_correct / T_incorrect) were calculated
441 from three trials at contrast 1 and 0.5 (Figure 6E). At 100% contrast, the OMR indices
442 were significantly reduced in *Gsk3α*$^{f/+}$*β*$^{f/f}$;*α-Cre* mice compared to controls at 0.05,
443 0.15 and 0.25 cycles per degree (cpd). The maximum OMR index was observed at
444 0.15 cpd in controls whereas it reached its maximum at 0.1 in *Gsk3α*$^{f/+}$*β*$^{f/f}$;*α-Cre* mice.
445 At 50% contrast, the OMR indices were also significantly reduced in *Gsk3α*$^{f/+}$*β*$^{f/f}$;*α-*
446 *Cre* mice compared to controls but to a larger extend between 0.05 and 0.3 cpd. The
447 maximum OMR index was observed at 0.15 cpd in both controls and *Gsk3α*$^{f/+}$*β*$^{f/f}$;*α-*
448 *Cre* mice. Altogether, these results demonstrate an impaired OMR in *Gsk3α*$^{f/+}$*β*$^{f/f}$;*α-*
449 *Cre* mice. These data, together with our transcriptomic and axonal projections
450 analyses, suggest that at least a subset of dRGCs expressing only one allele of
451 *Gsk3α* are DS-RGCs.
452

453 ## DISCUSSION

454 In this study, we report that complete loss of GSK3 in retinal progenitors leads
455 to microphthalmia in adult mice with severe morphological defects Such a severe
456 phenotype was not observed anymore when only one *Gsk3α* or *Gsk3β* allele was
457 expressed, confirming the functional redundancy of these two genes. Our results
458 implicate that the kinase GSK3 as the first reported determinant of dRGCs
459 determinant during retinal histogenesis. We show that mouse retinas with only one
460 allele of *Gsk3* exhibit an excessive number of dRGCs. The concomitant large
461 increase of axonal projections to the ipsilateral MTN, our RNA-Seq data and
462 optomotor response tests, have led us to propose that these dRGCs are involved in
463 the detection of image motion direction.

eNeuro Accepted Manuscript

464 In pigmented wild-type mouse retina, dRGCs in the INL are a very rare and
465 poorly-described type of cells, which represent only 2% of RGCs (Li et al., 2012;
466 Moore et al., 2002). It is therefore striking that dRGC number increases up to 20% of
467 RGCs when a single copy of *Gsk3α* is present in retinal progenitors. To our
468 knowledge, such a high number of dRGCs has never been reported in a
469 transgenic/mutant animal. A previous study hypothesized that dRGCs are misplaced
470 in the INL due to an ontogenic aberration rather than representing an independent
471 class of RGCs (Fite et al., 1981; Krause et al., 2014). Indeed, differential cell
472 adhesion plays a key role in sorting and migration of retinal cells in their appropriate
473 layers, especially for RGCs. One can therefore hypothesize that enhanced dRGCs in
474 mice with a single copy of *Gsk3* is the consequence of increased aberration events.
475 This hypothesis could be supported by our RNA-Seq data showing the upregulation
476 of genes coding for collagen subunits (*Col18a1*, *Col4a3*, *Col9a1*, *Col9a2*) and
477 extracellular matrix proteins in $Gsk3\alpha^{f/+}\beta^{f/f}$;*α-Cre* retina, which could favor migration
478 defects. Noticeably, if it were the case, the increase in dRGCs should be
479 accompanied by a decrease in oRGCs. However, we found that the number of oRGC
480 in the GCL is unaltered, strongly suggesting that RGCs in the INL of mice with a
481 single copy of *Gsk3* represent a specific subtype of RGCs. In support with this,
482 topographic and quantitative analysis of RGCs in albinos and pigmented rats indicate
483 that dRGCs are not misplaced by ontogenic mistakes but indeed represent a specific
484 subpopulation of RGCs (Nadal-NicolÃ¡s et al., 2014). GSK3β is involved in neural cell
485 fate decision by controlling the timing of the activity of bHLH transcription factors,
486 such as NeuroD or Neurog2 (Karten et al., 1977). If dRGCs are not produced
487 following ontogenic aberrations but are instead determined by a proper genetic
488 program, it would be interesting to identify transcription factors involved and seek for
489 any regulation by GSK3 kinases. Along this line, further studies would allow to better

eNeuro Accepted Manuscript

490 understand if the excess of dRGCs is only due to an expanded pool of normally
491 occurring dRGCs or if their presence is also a consequence of an aberrant migration
492 during retinal development when GSK3s are not fully active. New sequencing
493 technology such as single cell RNA-Seq would definitively be an asset to shed more
494 light on specific markers for dRGCs and to identify key players of dRGC
495 specification/differentiation. As a distinct cell type, scRNA-seq analysis following high
496 depth sequencing should highlight a distinct cell cluster in tSNE plots in retina with
497 only one *Gsk3α* allele expressed corresponding to dRGCs. The interest and power of
498 such approach has already been demonstrated for RGC characterization (Rheaume
499 et al., 2018). Whole transcriptome analysis at early time points when RGCs are
500 produced might also complete such analysis.
501 In reptiles, amphibians and birds, only dRGCs project into the MTN, whereas
502 in mammals only oRGCs have been reported as projecting into the MTN (Mouritsen
503 et al., 2004). Our results obtained from anterograde labeling clearly demonstrated a
504 large increase in ipsilateral MTN projections in absence of *Gsk3β*, whereas it was
505 absent or very dim in control animals. Although this strongly suggests that excess
506 dRGCs in mutant mice are causing this phenotype, we cannot exclude the possibility
507 that mutant oRGCs also participate to these ipsilateral MTN projections. However,
508 contralateral projections did not seem to be affected. Noticeably however, it would be
509 challenging to observe an increase in dRGC projections into the other areas already
510 strongly labeled using our anterograde labeling method, especially into the dLGN or
511 SC. We can speculate that the low number of ipsilateral MTN projections in the
512 control condition reflects the low number of dRGCs present in the WT retina and
513 could therefore explain why such result had not been described so far. Altogether,
514 our results strongly suggest that dRGCs may primarily project into the ipsilateral
515 MTN. In mice, it has been shown by retrograde labeling from the superior colliculus

eNeuro Accepted Manuscript

516 (SC), which receive large amount of RGC projections, that dRGCs/oRGCs project to
517 one or both SCs (Nießner et al., 2016). Although challenging, similar experiments,
518 *i.e.* fluorescent dye injection into the ipsilateral MTN, may allow us to discriminate
519 whether the increased signal in absence of *Gsk3β* originates only from dRGCs and
520 whether these cells also project into this area in WT retina. In regards to our results, it
521 is still unclear whether GSK3 function is to limit the number of dRGCs and actively
522 regulates their correct projection to the contralateral MTN or if GSK3 function is
523 limited to tightly controlling of dRGC number, which project thereafter to the ipsilateral
524 MTN on a GSK3-independent manner.

525 Given the very low percentage of dRGCs in the control retina, their function is
526 poorly studied in mammals. In contrast, dRGC function, projections and topography
527 have been extensively investigated in bird and reptile retina (Nießner et al., 2016). In
528 birds, cryptochrome-expressing dRGCs are used as a magnetic compass for
529 orientation (Pang and Wu, 2011). In European Robin birds, *Erithacus rubecula,* a low
530 number of dRGCs have been identified but specifically express Cryptochrome 1b
531 only during nocturnal migration period (Pang and Wu, 2011). In rodents, retrograde
532 labeling from the optic nerve led to the identification of 16 classes of dRGCs based
533 on their ramification levels of their dendrites as well as the dendritic field size (Giolli et
534 al., 2006; Yonehara et al., 2009). Based on dRGC dendrite projections into the IPL, it
535 has been proposed that most dRGCs in WT retina are functionally more involved in
536 retinal OFF light pathways (Simpson, 1984; Yonehara et al., 2009). Similar methods
537 applied to $Gsk3\alpha^{f/+}\beta^{f/f}$;*α-Cre* retina should shed more light on dRGC function and
538 establish whether all the different classes are present.

539 As part of the AOS, the MTN receives afferent signal from the eye and sends
540 efferent signal to motor neurons controlling the position of the eye. As such,
541 optokinetic reflex relies on direction specific retinal projections to the AOS. Neurons

eNeuro Accepted Manuscript

542 of the dorsal terminal nucleus (DTN) codes for horizontal stimulus whereas neurons
543 of the MTN codes for vertical stimulus (Nadal-NicolÃ¡s et al., 2014). Therefore, the
544 direction of image motion relies on DS-RGCs in the retina. The alteration the OMR in
545 *Gsk3α$^{f/+}$β$^{f/f}$;α-Cre* mice, support the hypothesis that some of the supernumerary
546 dRGCs are indeed related to motion detection. Although the number of dRGCs was
547 drastically increased, the OMR was not increased but at the contrary reduced. Such
548 result might be caused by the higher number of projections to the ipsilateral side
549 instead of the contralateral one, leading to an alteration of the neuronal circuit
550 regulating the OMR (Nadal-NicolÃ¡s et al., 2014). We also identified in *Gsk3α$^{f/+}$β$^{f/f}$;α-*
551 *Cre* and control retinas a small subset of dRGCs, which are positive for the
552 transcription factors Tbr2 and Foxp2, the markers for non-image-forming RGCs and
553 DS-RGCs respectively (Marquardt et al., 2001). Together with the transcriptomic data
554 (upregulation of genes such as *Cartpt* expressed in DS-RGCs), these results provide
555 strong evidence suggesting that the large number of dRGCs in *Gsk3α$^{f/+}$β$^{f/f}$;α-Cre*
556 retina might indeed be DS-RGCs projecting into the MTN. It has been recently
557 proposed that dRGCs might be also involved in predator detection by integrating
558 overhead visual information (Roger et al., 2010). Using suitable and complementary
559 visual tests, our genetic model could be highly valuable to complete the functional
560 identification of the dRGCs in visual process.

561 Overall, our results demonstrate a critical role of GSK3 in stringently regulating
562 the number of a rare type of dRGCs, which has been poorly described as yet. *Gsk3*
563 mutant mice, with a large number of dRGCs in their retina, offer a unique and
564 powerful model system to further study the embryonic origin, synaptic connections
565 and visual function of dRGCs in mammals.
566

eNeuro Accepted Manuscript

ACKNOWLEDGEMENT

We are grateful to Dr. Jim Woodgett for providing the *Gsk3* floxed lines and Tudor Badea and Peter Gruss for the alpha-Cre line. We would also like also to thank Elodie-Kim Grellier, Yide Mi, and Jessica Gumerson for their help with mouse colonies and technical support.

FUNDING SOURCES

This research was supported by the CNRS, Retina France and by the Intramural Research Program of the National Eye Institute (EY000450 and EY000546). EK was supported by the Ernst Ludwig Ehrlich Studienwerk.

AUTHOR'S CONTRIBUTION

E.K., R.J.V., C.H., designed and performed the experiments and analyzed the data, S.L. L.T. and P.S. performed the experiments and analyzed the data, A.C. designed the experiments, analyzed the data and revised the manuscript, M.P., A.S., J.E.R. designed the study, analyzed the data, wrote the manuscript with the help of E.K. R.J.V and C.H. J.E.R supervised the study.

REFERENCES

Balkema GW, DrÄger UC (1990) Origins of uncrossed retinofugal projections in normal and hypopigmented mice. Visual Neuroscience 4:595–604.

Bejarano-Escobar R, Álvarez-Hernán G, Morona R, González A, Martín-Partido G, Francisco-Morcillo J (2015) Expression and function of the LIM-homeodomain transcription factor Islet-1 in the developing and mature vertebrate retina. Experimental Eye Research.

Belle M, Godefroy D, Couly G, Malone SA, Collier F, Giacobini P, Chédotal A (2017) Tridimensional Visualization and Analysis of Early Human Development. Cell 169:161-173.e12.

595 Belle M, Godefroy D, Dominici C, Heitz-Marchaland C, Zelina P, Hellal F, Bradke F,
596 Chédotal A (2014) A simple method for 3D analysis of immunolabeled axonal tracts in a
597 transparent nervous system. Cell reports 9:1191–201.
598 Buhl EH, Dann JF (1988) Morphological diversity of displaced retinal ganglion cells in the
599 rat: A lucifer yellow study. Journal of Comparative Neurology 269:210–218.
600 Chen Y, Mccarthy D, Robinson M, Smyth GK (2015) edgeR : differential expression analysis
601 of digital gene expression data User ' s Guide.
602 Cole AR (2012) GSK3 as a Sensor Determining Cell Fate in the Brain. Frontiers in Molecular
603 Neuroscience 5:1–10.
604 Cook JE, Podugolnikova TA (2001) Evidence for spatial regularity among retinal ganglion
605 cells that project to the accessory optic system in a frog, a reptile, a bird, and a mammal.
606 Visual Neuroscience 18:289–297.
607 Dobin A, Davis CA, Schlesinger F, Drenkow J, Zaleski C, Jha S, Batut P, Chaisson M,
608 Gingeras TR (2013) STAR: Ultrafast universal RNA-seq aligner. Bioinformatics 29:15–
609 21.
610 Doble BW, Patel S, Wood GA, Kockeritz LK, Woodgett JR (2007) Functional redundancy of
611 GSK-3alpha and GSK-3beta in Wnt/beta-catenin signaling shown by using an allelic
612 series of embryonic stem cell lines. Developmental cell 12:957–71.
613 Doble BW, Woodgett JR (2003) GSK-3: Tricks of the trade for a multi-tasking kinase.
614 Journal of Cell Science.
615 Doi M, Imatani H, Sasoh M, Uji Y, Yamamura H (1994) Displaced retinal ganglion cells in
616 the Chinese hamster. Japanese journal of ophthalmology 38:139–43.
617 Dräger UC, Olsen JF (1980) Origins of crossed and uncrossed retinal projections in
618 pigmented and albino mice. Journal of Comparative Neurology 191:383–412.
619 Eom TY, Jope RS (2009) Blocked Inhibitory Serine-Phosphorylation of Glycogen Synthase
620 Kinase-3α/β Impairs In Vivo Neural Precursor Cell Proliferation. Biological Psychiatry
621 66:494–502.
622 Espinosa L, Inglés-Esteve J, Aguilera C, Bigas A (2003) Phosphorylation by glycogen
623 synthase kinase-3β down-regulates Notch activity, a link for Notch and Wnt pathways.
624 Journal of Biological Chemistry 278:32227–32235.
625 Fite K v, Brecha N, Karten HJ, Hunt SP (1981) Displaced ganglion cells and the accessory
626 optic system of pigeon. The Journal of comparative neurology 195:279–88.
627 Fu X, Sun H, Klein WH, Mu X (2006) B-Catenin Is Essential for Lamination But Not
628 Neurogenesis in Mouse Retinal Development. Developmental Biology 299:424–437.
629 Galli-Resta L, Ensini M (1996) An intrinsic time limit between genesis and death of
630 individual neurons in the developing retinal ganglion cell layer. Journal of Neuroscience
631 16:2318–2324.
632 Giolli RA, Blanks RHI, Lui F (2006) The accessory optic system: basic organization with an
633 update on connectivity, neurochemistry, and function. Progress in brain research
634 151:407–40.
635 Golpich M, Amini E, Hemmati F, Ibrahim NM, Rahmani B, Mohamed Z, Raymond AA,
636 Dargahi L, Ghasemi R, Ahmadiani A (2015) Glycogen synthase kinase-3 beta (GSK-3β)
637 signaling: Implications for Parkinson's disease. Pharmacological Research.
638 Hamon A, García-García D, Ail D, Bitard J, Chesneau A, Dalkara D, Locker M, Roger JE,
639 Perron M (2019) Linking YAP to Müller Glia Quiescence Exit in the Degenerative
640 Retina. Cell reports 27:1712-1725.e6.
641 Hur E-M, Zhou F-Q (2010) GSK3 signalling in neural development. Nature reviews
642 Neuroscience 11:539–551.
643 Jacobs KM, Bhave SR, Ferraro DJ, Jaboin JJ, Hallahan DE, Thotala D (2012) GSK-3β: A
644 Bifunctional Role in Cell Death Pathways. International journal of cell biology
645 2012:930710.

eNeuro Accepted Manuscript

eNeuro Accepted Manuscript

646 Jin YH, Kim H, Oh M, Ki H, Kim K (2009) Regulation of Notch1/NICD and Hes1
647 expressions by GSK-3α/β. Molecules and Cells 27:15–19.
648 Karten HJ, Fite K v., Brecha N (1977) Specific projection of displaced retinal ganglion cells
649 upon the accessory optic system in the pigeon (Columbia livia). Proceedings of the
650 National Academy of Sciences of the United States of America 74:1753–1756.
651 Kay JN, de la Huerta I, Kim IJ, Zhang Y, Yamagata M, Chu MW, Meister M, Sanes JR
652 (2011) Retinal ganglion cells with distinct directional preferences differ in molecular
653 identity, structure, and central projections. Journal of Neuroscience 31:7753–7762.
654 Kim W-Y, Wang X, Wu Y, Doble BW, Patel S, Woodgett JR, Snider WD (2009) GSK-3 is a
655 master regulator of neural progenitor homeostasis. Nature neuroscience 12:1390–1397.
656 Krause M, Distler C, Hoffmann KP (2014) Retinal ganglion cells projecting to the accessory
657 optic system in optokinetic blind albinotic rats are direction-selective. European Journal
658 of Neuroscience 40:2274–2282.
659 Kremer A (2011) GSK3 and Alzheimer's disease: facts and fiction…. Frontiers in Molecular
660 Neuroscience 4:1–10.
661 Kretschmer F, Kretschmer V, Kunze VP, Kretzberg J (2013) OMR-arena: Automated
662 measurement and stimulation system to determine mouse visual thresholds based on
663 optomotor responses. PLoS ONE 8:78058.
664 Kretschmer F, Sajgo S, Kretschmer V, Badea TC (2015) A system to measure the Optokinetic
665 and Optomotor response in mice. Journal of Neuroscience Methods 256:91–105.
666 Li DW, Liu ZQ, Chen W, Yao M, Li GR (2014) Association of glycogen synthase kinase-3β
667 with Parkinson's disease (Review). Molecular Medicine Reports.
668 Li S, Mattar P, Zinyk D, Singh K, Chaturvedi C-P, Kovach C, Dixit R, Kurrasch DM, Ma Y-
669 C, Chan JA, Wallace V, Dilworth FJ, Brand M, Schuurmans C (2012) GSK3 temporally
670 regulates neurogenin 2 proneural activity in the neocortex. The Journal of neuroscience :
671 the official journal of the Society for Neuroscience 32:7791–805.
672 Liao Y, Smyth GK, Shi W (2014) FeatureCounts: An efficient general purpose program for
673 assigning sequence reads to genomic features. Bioinformatics 30:923–930.
674 Livak KJ, Schmittgen TD (2001) Analysis of relative gene expression data using real-time
675 quantitative PCR and the 2-ΔΔCT method. Methods 25:402–408.
676 Marcus EA, Kintner C, Harris W (1998) The role of GSK3β in regulating neuronal
677 differentiation in Xenopus laevis. Molecular and Cellular Neurosciences 12:269–280.
678 Marquardt T, Ashery-Padan R, Andrejewski N, Scardigli R, Guillemot F, Gruss P (2001)
679 Pax6 is required for the multipotent state of retinal progenitor cells. Cell 105:43–55.
680 Maurer U, Preiss F, Brauns-Schubert P, Schlicher L, Charvet C (2014) GSK-3 - at the
681 crossroads of cell death and survival. Journal of Cell Science 127:1369–1378.
682 Medina M, Garrido JJ, Wandosell FG (2011) Modulation of GSK-3 as a Therapeutic Strategy
683 on Tau Pathologies. Frontiers in Molecular Neuroscience 4:1–10.
684 Moore KB, Schneider ML, Vetter ML (2002) Posttranslational mechanisms control the timing
685 of bHLH function and regulate retinal cell fate. Neuron 34:183–195.
686 Mouritsen H, Janssen-Bienhold U, Liedvogel M, Feenders G, Stalleicken J, Dirks P, Weiler R
687 (2004) Cryptochromes and neuronal-activity markers colocalize in the retina of
688 migratory birds during magnetic orientation. Proceedings of the National Academy of
689 Sciences of the United States of America 101:14294–9.
690 Nadal-Nicolás FM, Jiménez-López M, Salinas-Navarro M, Sobrado-Calvo P, Alburquerque-
691 Béjar JJ, Vidal-Sanz M, Agudo-Barriuso M (2012) Whole Number, Distribution and Co-
692 Expression of Brn3 Transcription Factors in Retinal Ganglion Cells of Adult Albino and
693 Pigmented Rats. PLoS ONE 7:e49830.
694 Nadal-NicolÃ¡s FM, Salinas-Navarro M, JimÃ©nez-LÃ³pez M, Sobrado-Calvo P, Villegas-
695 PÃ©rez MP, Vidal-Sanz M, Agudo-Barriuso M (2014) Displaced retinal ganglion cells
696 in albino and pigmented rats. Frontiers in Neuroanatomy 8:1–21.

eNeuro Accepted Manuscript

697 Nießner C, Gross JC, Denzau S, Peichl L, Fleissner G, Wiltschko W, Wiltschko R (2016)
698 Seasonally changing cryptochrome 1b expression in the retinal ganglion cells of a
699 migrating passerine bird. PLoS ONE 11:e0150377.
700 Ouchi Y, Baba Y, Koso H, Taketo MM, Iwamoto T, Aburatani H, Watanabe S (2011) β-
701 Catenin signaling regulates the timing of cell differentiation in mouse retinal progenitor
702 cells. Molecular and Cellular Neuroscience 46:770–780.
703 Pachenari N, Kiani S, Javan M (2017) Inhibition of glycogen synthase kinase 3 increased
704 subventricular zone stem cells proliferation. Biomedicine & pharmacotherapy =
705 Biomedecine & pharmacotherapie 93:1074–1082.
706 Pang J-J, Wu SM (2011) Morphology and immunoreactivity of retrogradely double-labeled
707 ganglion cells in the mouse retina. Investigative ophthalmology & visual science
708 52:4886–96.
709 Pérezleón JA, Osorio-Paz I, Francois L, Salceda R (2013) Immunohistochemical localization
710 of glycogen synthase and GSK3β: Control of glycogen content in retina. Neurochemical
711 Research 38:1063–1069.
712 Rheaume BA, Jereen A, Bolisetty M, Sajid MS, Yang Y, Renna K, Sun L, Robson P,
713 Trakhtenberg EF (2018) Single cell transcriptome profiling of retinal ganglion cells
714 identifies cellular subtypes. Nature Communications 9.
715 Rodriguez AR, de Sevilla Müller LP, Brecha NC (2014) The RNA binding protein RBPMS is
716 a selective marker of ganglion cells in the mammalian retina. Journal of Comparative
717 Neurology 522:1411–1443.
718 Roger JEJE, Nellissery J, Kim DSDSDS, Swaroop A (2010) Sumoylation of bZIP
719 transcription factor NRL modulates target gene expression during photoreceptor
720 differentiation. Journal of Biological Chemistry 285:25637–25644.
721 Roger JEJEE, Ranganath K, Zhao L, Cojocaru RIRIIRI, Brooks M, Gotoh N, Veleri S,
722 Hiriyanna A, Rachel RARARA, Campos MMMMM, Fariss RNRNN, Wong WTTWT,
723 Swaroop A (2012) Preservation of cone photoreceptors after a rapid yet transient
724 degeneration and remodeling in cone-only Nrl-/- mouse retina. J Neurosci 32:528–541.
725 Rousso DL, Qiao M, Kagan RD, Yamagata M, Palmiter RD, Sanes JR (2016) Two Pairs of
726 ON and OFF Retinal Ganglion Cells Are Defined by Intersectional Patterns of
727 Transcription Factor Expression. Cell reports 15:1930–44.
728 S H, H W (2000) Immunocytochemical analysis of the mouse retina. The Journal of
729 comparative neurology 424:1–23.
730 Sajgo S, Ghinia MG, Brooks M, Kretschmer F, Chuang K, Hiriyanna S, Wu Z, Popescu O,
731 Badea TC (2017) Molecular codes for cell type specification in Brn3 retinal ganglion
732 cells. Proceedings of the National Academy of Sciences of the United States of America
733 114:E3974–E3983.
734 Sato C, Iwai-Takekoshi L, Ichikawa Y, Kawasaki H (2017) Cell type-specific expression of
735 FoxP2 in the ferret and mouse retina. Neuroscience Research 117:1–13.
736 Shimizu T, Kagawa T, Inoue T, Nonaka A, Takada S, Aburatani H, Taga T (2008) Stabilized
737 beta-catenin functions through TCF/LEF proteins and the Notch/RBP-Jkappa complex to
738 promote proliferation and suppress differentiation of neural precursor cells. Molecular
739 and cellular biology 28:7427–41.
740 Simpson JI (1984) The Accessory Optic System. Annual Review of Neuroscience 7:13–41.
741 Sweeney NT, James KN, Nistorica A, Lorig-Roach RM, Feldheim DA (2019) Expression of
742 transcription factors divides retinal ganglion cells into distinct classes. Journal of
743 Comparative Neurology 527:225–235.
744 Sweeney NT, Tierney H, Feldheim DA (2014) Tbr2 is required to generate a neural circuit
745 mediating the pupillary light reflex. The Journal of neuroscience : the official journal of
746 the Society for Neuroscience 34:5447–53.

eNeuro Accepted Manuscript

747 Wall DS, Mears AJ, McNeill B, Mazerolle C, Thurig S, Wang Y, Kageyama R, Wallace VA
748 (2009) Progenitor cell proliferation in the retina is dependent on Notch-independent
749 Sonic hedgehog/Hes1 activity. Journal of Cell Biology 184:101–112.
750 Walter W, Sánchez-Cabo F, Ricote M (2015) GOplot: an R package for visually combining
751 expression data with functional analysis. Bioinformatics (Oxford, England) 31:2912–4.
752 Wang B, Li Y (2006) Evidence for the direct involvement of βTrCP in Gli3 protein
753 processing. Proceedings of the National Academy of Sciences of the United States of
754 America 103:33–38.
755 Yonehara K, Ishikane H, Sakuta H, Shintani T, Nakamura-Yonehara K, Kamiji NL, Usui S,
756 Noda M (2009) Identification of retinal ganglion cells and their projections involved in
757 central transmission of information about upward and downward image motion. PLoS
758 ONE 4:e4320.
759 Young RW (1984) Cell death during differentiation of the retina in the mouse. Journal of
760 Comparative Neurology 229:362–373.
761 Zhou Y, Zhou B, Pache L, Chang M, Khodabakhshi AH, Tanaseichuk O, Benner C, Chanda
762 SK (2019) Metascape provides a biologist-oriented resource for the analysis of systems-
763 level datasets. Nature Communications 10:1523.
764

765

766 ## FIGURE AND EXTENDED DATA LEGENDS

767 **Figure 1. Developmental defects and microphthalmia in *Gsk3*-deficient retina**
768 **with aberrant nuclear translocation of β-catenin, a key effector of the Wnt**
769 **canonical pathway.** (A) Immunohistochemistry (IHC) of E12.5 retina from *Gsk3α$^{f/f}$β$^{f/f}$*
770 mice expressing or not α-Cre using a pan-GSK3 antibody (green) shows efficient
771 deletion at the periphery where the Cre expression has been previously reported
772 (delimited by dashed-line) Scale bar: 100 μm. (B) Hematoxylin and eosin (H&E)
773 staining on methacrylate sections at E12.5, E14.5 and P2 reveals large retinal
774 morphogenesis defects in *Gsk3α$^{f/f}$β$^{f/f}$;α-Cre* with blood invasion into the eyeball
775 (showed by white arrow). L, Lens; NR, neural retina. Scale bar: 100 μm at E12.5 and
776 E14.5. 500 μm at P2. For the magnification of P14.5, scale bar: 50 μm.

777

778 **Figure 2. One allele of either *Gsk3α* or *Gsk3β* is sufficient for the development**
779 **of a functional retina.** (A) Immunoblot analysis of protein extracts from 2-month-old
780 animals with different combination of *Gsk3α* and *Gsk3β* floxed alleles (*Gsk3α$^{f/f}$β$^{+/+}$*,
781 *Gsk3α$^{+/+}$β$^{f/f}$*, *Gsk3α$^{f/+}$β$^{f/f}$* or *Gsk3α$^{f/f}$β$^{f/+}$*) with or without *Cre* recombinase using anti-
782 panGSK3 antibody (recognizing both isoforms) reveals decreased expression of
783 GSK3α or GSK3*β* (arrowheads). *α*-Tubulin is used as loading control. (B) IHC on 2-
784 month-old retinal sections from control and *Gsk3α$^{f/+}$β$^{f/f}$*; *α-Cre* retinas with or without
785 Cre recombinase using anti-GSK3β antibody (red) showing ubiquitous *Gsk3β*
786 expression in all retinal layers, whereas its expression is lost in the Cre-expressing
787 retina. (C) Expression of only one *Gsk3* allele (*Gsk3α*) is sufficient for proper
788 photoreceptor development. IHC using anti-Rhodopsin (Rho, red) and anti-Cone
789 arrestin (Arr3, red) antibodies to label rod and cone photoreceptors, respectively. (D)
790 Expression of only one *Gsk3* allele (*Gsk3α*) is sufficient for proper interneuron

eNeuro Accepted Manuscript

791 development. IHC using anti-Calretinin (Calr, green) and anti-Calbindin (Calb, red)
792 antibodies to label horizontal and amacrine cells, respectively. (B-D) onl, outer
793 nuclear layer; inl, inner nuclear layer; gcl, ganglion cell layer. Scale bar: 20μm. (E, F)
794 Electroretinogram (ERG) recording in 2-month-old *Gsk3*$\alpha^{f/+}\beta^{f/f}$;*α-Cre* animals and
795 littermate controls. Photopic (cones) (E) and scotopic (rods) (F) response in
796 *Gsk3*$\alpha^{f/+}\beta^{f/f}$;*α-Cre* animals are similar to controls. Mean ± SEM intensity response
797 curves of a- and b-wave responses averaged from 8 biological replicates of each
798 genotype.
799

800 **Figure 3. Gradual loss of *Gsk3α* and/or *Gsk3β* leads to an increased number of**
801 **Brn3a-positive retinal ganglion cells displaced in the inner nuclear layer (INL)**
802 **of adult retina.** (A) Brn3a (red) and NF68 (green) IHC on 2-month-old *Gsk3*$\alpha^{f/+}\beta^{f/f}$; *α-*
803 *Cre* mouse retina reveals the presence of supernumerary displaced retinal ganglion
804 cells (dRGCs, arrows) in the INL of *Gsk3*$\alpha^{f/+}\beta^{f/f}$; *α-Cre* compared to littermate
805 controls. Top panel represents control retinas, middle panel a peripheral retinal area,
806 and bottom panel a more central area. Scale bar: 20 μm. (B) dRGCs send their
807 axons into the optic nerve. Visualization of dRGCs after 3D reconstruction of 2-
808 month-old flat mounted retina of control and *Gsk3*$\alpha^{f/+}\beta^{f/f}$; *α-Cre* animals following
809 retrograde labeling with Rhodamin-Dextran applied onto the optic nerve. inl: inner
810 nuclear layer, gcl: ganglion cell layer. (C) Gradual loss of *Gsk3α* and *Gsk3β* alleles
811 (*Gsk3*$\alpha^{f/f}\beta^{+/+}$, *Gsk3*$\alpha^{+/+}\beta^{f/f}$, *Gsk3*$\alpha^{f/+}\beta^{f/f}$ or *Gsk3*$\alpha^{f/f}\beta^{f/+}$) leads to a gradual increase of
812 Brn3a-positive RGCs located to the INL, with the highest number observed in
813 *Gsk3*$\alpha^{f/+}\beta^{f/f}$; *α-Cre* animals. ~~Left~~ Histograms represent counting of the total number of
814 Brn3a-positive cells per section located in the GCL (*left panel*) or in the INL (*middle*
815 *panel*). Right histogram represents the percentage of the dRGCs among the total
816 number of Brn3a-positive cells per section for each combination. Mean ± SEM values

eNeuro Accepted Manuscript

eNeuro Accepted Manuscript

817 are presented from 4 biological replicates. A nonparametric Mann-Whitney U test
818 was applied, * indicates $P \leq 0.05$. (D) Brn3a (red) and Rbpms (green) IHC on 2-
819 month-old mouse retina reveal the co-expression of these two RGC markers
820 (dRGCs, arrows) in the INL of both *Gsk3α*$^{f/+}$*β*$^{f/f}$*; α-Cre* dRGCs and in littermate
821 controls. Scale bar: 20 μm. (E) Flat mounted retina from *Gsk3α*$^{f/+}$*β*$^{f/f}$*; α-Cre* and
822 littermate controls labelled with anti-Rbpms antibody demonstrated the large number
823 of Rbpms-positive dRGCs in the INL of *Gsk3α*$^{f/+}$*β*$^{f/f}$*; α-Cre* mice. See Extended Data
824 Figure 3-1 for Islet1 and Rbpms co-localization used to complete dRGC
825 characterization and the repartition of the dRGCs in the retina. See Extended Data
826 Figure 3-2 showing that Brn3a-positive dRGCs are not positive for amacrine or
827 horizontal cell markers.
828

829 **Figure 4. dRGCs are produced in the same differentiation wave as oRGC**
830 **located in the GCL.** (A) EdU- (green) and Brn3a-positive cells (red) were found both
831 in the GCL and in the INL of 30-days old *Gsk3α*$^{f/+}$*β*$^{f/f}$; *α-Cre* animals after a single
832 injection of EdU at E12.5. (B) Percentage of EdU- and Brn3a-positive cells located
833 either in the GCL or in the INL among total number of Brn3a-positive cells. Mean ±
834 SEM values are presented from 3-4 biological replicates. A nonparametric Mann-
835 Whitney U test was applied, ns: not significant (C) Brn3a (*red*) and NF68 (green)
836 immunostaining on P0 mouse retina revealed that a large number of dRGCs were
837 already present in *Gsk3α*$^{f/+}$*β*$^{f/f}$*; α-Cre* but they were fewer in littermate controls *(*white
838 arrows*)*. (D) Left stacked histogram represents counting of the total number of Brn3a-
839 positive cells per section located in the GCL (white bars) and in the INL (black bars)
840 of *Gsk3α*$^{f/+}$*β*$^{f/f}$*; α-Cre* retina. Right histogram represents the percentage of the dRGCs
841 among the total number of Brn3a-positive cells per section. Mean ± SEM values are
842 presented from 6 biological replicates. A nonparametric Mann-Whitney U test was

eNeuro Accepted Manuscript

843 applied, ** indicates $P \leq 0.01$. inl, inner nuclear layer; gcl, ganglion cell layer. Scale
844 bar: 20μm.
845
846 **Figure 5. Lack of Gsk3β results in RGC projections into the ipsilateral Medial**
847 **Terminal Nucleus.** (A) All panels are light sheet fluorescence microscopy of solvent-
848 cleared adult brain from control, *Gsk3α$^{f/f}$β$^{+/+}$; α-Cre*, *Gsk3α$^{+/+}$β$^{f/f}$; α-Cre* and
849 *Gsk3α$^{f/+}$β$^{f/f}$; α-Cre* animals after intravitreal injection of CTB coupled to either an
850 Alexa-555 or -647. Ipsilateral projections of RGCs into the MTN was observed in the
851 absence of *Gsk3β* expression. SC, superior colliculus; NOT, nucleus of optic tract;
852 dLGN, dorsal lateral geniculate nucleus; vLGN, ventral lateral geniculate nucleus;
853 IGL, intergeniculate leaflet; OPT, Olivary Pretectal Nucleus; dMTN, dorsal medial
854 terminal nucleus; MTN, medial terminal nucleus; vMTN, ventral medial terminal
855 nucleus; OT, Optic tract; SCN, suprachiasmatic nucleus; ON, optic nerve. Scale bar:
856 1mm; * indicates the ipsilateral MTN. (B) Quantification of the signal intensity ratio
857 between ipsilateral and contralateral MTN in controls and *Gsk3* mutants (including
858 *Gsk3α$^{f/f}$β$^{+/+}$; α-Cre*, *Gsk3α$^{+/+}$β$^{f/f}$; α-Cre*, and *Gsk3α$^{f/+}$β$^{f/f}$; α-Cre*). A nonparametric
859 Mann-Whitney U test was applied, ns: non-significant, ** $P \leq 0.01$. See Extended
860 Data Figure 5-1 for co-staining of the CTB-positive cells with Brn3a and NF68.
861
862 **Figure 6. Whole transcriptome meta-analysis suggests that dRGC in**
863 ***Gsk3α$^{f/+}$β$^{f/f}$*; *α-Cre* retina are direction-selective ganglion cells.** (A) Volcano plot
864 representation of differentially expressed genes between *Gsk3αf/+βf/f; α-Cre* and
865 control retina plotted on the x-axis (log2 scale). FDR adjusted significance is plotted
866 on the y-axis. Orange and blue dots: significantly up-regulated and down-regulated
867 genes in *Gsk3α$^{f/+}$β$^{f/f}$; α-Cre* retina, respectively. Vertical dashed lines represent
868 FC=1.5. Horizontal dashed line represents FDR=0.05. (B) Chord plot representation

869 of DEGs related to GO annotations belonging to either molecular functions (MF) or
870 biological process (BP). Overlaps in GO annotation amongst genes within each
871 category are visualized. * correspond to genes expressed in previously published
872 purified RGCs (blue, slightly expressed genes in RGCs between 1 and 5 FPKM; red,
873 highly expressed genes in RGCs more than 5 FPKM). (C) RT-qPCR validation of
874 selected DEGs identified by RNA-seq analysis. Differential expression analysis by
875 RT-qPCR of *Cartpt, Th, Epha2, Cplx1, Chrna5, Chrna2, Chrna7, Chrnb4* in
876 *Gsk3α*$^{f/+}$*β*$^{f/f}$*; α-Cre* retina at 2-months of age, relative to littermate control retina levels.
877 All values are expressed as the Mean ± SEM from three biological replicates. A
878 nonparametric Mann-Whitney U test was applied, * indicates $P \leq 0.05$. (D) IHC on 2-
879 month-old mouse retina reveals the presence of a subset of dRGCs (Rbpms-positive
880 dRGCs, red) in *Gsk3α*$^{f/+}$*β*$^{f/f}$*; α-Cre* expressing either the transcription factor Tbr2
881 (grey) or Foxp2 (green). Arrows indicate Tbr2 and Rbpms-positive dRGCs;
882 arrowheads represent Foxp2 and Rbpms-positive dRGCs. onl, outer nuclear layer;
883 inl, inner nuclear layer; gcl, ganglion cell layer. Scale bar: 50 µm. (E) The mean OMR
884 indices (±SEM) are plotted as a function of spatial frequency for each genotype
885 (n=13 for *Gsk3α*$^{f/+}$*β*$^{f/f}$ and 18 for *Gsk3α*$^{f/+}$*β*$^{f/f}$*;α-Cre* genotype). The baseline (1; dashed
886 line) represents unspecific head movements and no response to the stimulus. OMR
887 at 100% and 50% contrast in *Gsk3α*$^{f/+}$*β*$^{f/f}$*; α-Cre* mice (dashed line) and controls
888 (black line). A Grubbs test was performed at 5% to remove outliers followed by 2-way
889 ANOVA, * indicates $P \leq 0.05$, ** indicates $P \leq 0.01$, *** indicates $P \leq 0.001$. See
890 Extended Data Figure 6-1 for the hierarchical clustering of the DEGs. See Extended
891 Data Figure 6-2 for pathway analysis results.
892
893 **EXTENDED DATA**

eNeuro Accepted Manuscript

eNeuro Accepted Manuscript

894 **Figure 3-1. dRGCs express the nuclear factor Islet-1.** (A) IHC on 2-month-old
895 mouse retina reveals that most dRGCs (Rbpms-positive dRGCs, white arrows, red)
896 in the INL of *Gsk3α$^{f/+}$β$^{f/f}$; α-Cre* and littermate controls were positive for Islet-1
897 (green), a marker expressed in the nuclei of ganglion cells, and of cholinergic
898 amacrine cells, ON-bipolar cells, and subpopulations of horizontal cells. onl, outer
899 nuclear layer; inl, inner nuclear layer; gcl, ganglion cell layer. Scale bar: 50 µm. (B)
900 Counting on flat mount of Rbpms- or Brn3a- positive cells located in the INL at the
901 dorsal, ventral, nasal and temporal part of control and *Gsk3α$^{f/+}$β$^{f/f}$;α-Cre* retina.
902 Histogram represents the number of Brn3a- or Rbpms-positive cells per field. Mean ±
903 SEM values are presented from 4 biological replicates.
904
905 **Figure 3-2. Brn3a-positive cells located in the INL of *Gsk3α$^{f/+}$β$^{f/f}$; α-Cre* retina**
906 **are dRGCs.** Brn3a-positive RGCs located in the INL of *Gsk3α$^{f/+}$β$^{f/f}$; α-Cre* retina do
907 not express markers of other INL neurons such as Choline-Acetyltransferase (Chat)
908 or Calbindin (Calb). onl, outer nuclear layer; inl, inner nuclear layer; gcl, ganglion cell
909 layer. Arrowheads indicates Brn3a-positive dRGCs. Scale bar: 20µm.
910
911 **Figure 5-1. Intravitreal injection of CTB labels dRGCs.** After intravitreal injection of
912 CTB coupled to an Alexa-555 (*red*) in *Gsk3α$^{f/+}$β$^{f/f}$; α-Cre* eye led to the labelling of
913 Brn3a- (green) and NF68-positive (*grey*) cells located in the INL. Scale bars: 20µm
914
915 **Figure 6-1. Hierarchical clustering of the identified differentially expressed**
916 **genes.** Hierarchical clustering representing the 111 DEGs (abs(FC)≥1.5; FDR≤0.05;
917 FPKM>1) between 2-month-old *Gsk3α$^{f/+}$β$^{f/f}$; α-Cre* retina and littermate control were
918 clustered by their Z-score. Each column for each genotype corresponds to one

919 sample. For both groups, triplicates were analyzed. Left panel corresponds to the
920 downregulated genes; Right panel corresponds to the upregulated genes.
921
922 **Figure 6-2. Identification of enriched pathways from DEGs identified in 2-**
923 **month-old *Gsk3α$^{f/+}$β$^{f/f}$; α-Cre* retina.** (A) Gene ontology (GO) annotations of DEGs
924 in *Gsk3α$^{f/+}$β$^{f/f}$; α-Cre* retina compared to littermate controls. Top over-represented
925 pathways for Biological process (BP), Molecular Function (MF), KEGG (Kyoto
926 Encyclopedia of Genes and Genomes) and TRRUST (Transcriptional Regulatory
927 Relationships Unrevealed by Sentence-based Text mining) were identified by
928 enrichment analysis using Metascape. (B) Circular visualization for BP and MF of GO
929 enrichment analysis. Down-regulated genes (blue dots) and up-regulated genes (red
930 dots) within each GO pathway are plotted based on logFC. Z-score bars indicate if an
931 entire GO category is more likely to be increased or decreased based on the genes
932 within it.
933
934
935
936
937
938
939
940
941
942
943
944

eNeuro Accepted Manuscript

eNeuro Accepted Manuscript

945
946
947
948
949
950 **Table 1. List of primary and secondary antibodies used for**
951 **immunohistochemistry (IF) and western blot (WB)**
952 **Primary antibodies**

ANTIGENE	HOST	SUPPLIER	REFERENCE	DILUTION (IF)	DILUTION (WB)
α-tubulin	mouse	SIGMA	T5168		1:200.000
GSK3α/β	mouse	Thermo Fisher Scientific	44-610	1:250	1:1000
GSK3β	mouse	BD	610201	1:250	
Brn3a	mouse	Santa Cruz	sc-8429	1:200	
Calbindin D-28k	rabbit	Swant	300	1:100	
Calretinin	mouse	EMD Millipore	MAB1568	1:1000	
Cone Arrestin	rabbit	EMD Millipore	AB15282	1:1000	
Rhodopsin	Mouse	Abcam	MAB5316	1:2000	
Tbr2	Rat	Ebioscience	14-4876	1 :300	
Foxp2	Goat	Santa Cruz	sc-21069	1 :1000	
Rbpms	Rabbit	PhosphoSolutions	1830-RBPMS	1 :400	
Chat	Goat	Millipore	AB144P	1 :100	

953

954 **Secondary antibodies**

ANTIGENE	HOST	SUPPLIER	REFERENCE	DILUTION
Alexa Fluor 555 anti-mouse IgG2A	goat	Thermo Fisher Scientific	A21127	1:1000
Alexa Fluor 555	goat	Thermo Fisher	A21147	1:1000

eNeuro Accepted Manuscript

anti-mouse IgG2B		Scientific		
Alexa Fluor 488 anti-rabbit	donkey	Thermo Fisher Scientific	A21206	1:1000
Alexa Fluor 488 anti-mouse IgG1	goat	Thermo Fisher Scientific	A21240	1:1000
Alexa Fluor 488 anti-rabbit	goat	Thermo Fisher Scientific	A21244	1:1000
HRP anti-mouse IgG	goat	Sigma-Aldrich	A4416	1:5000

Gene name	**Primer F**	**Primer R**
Cartpt	5'-TAAAGTTTGCGTTCCCCTCAG-3'	5'-CAACACCATTCGAGGCATTCT-3'
Th	5'-ACTATGCCTCTCGTATCCAGC-3'	5'-CGGATGGTGTGAGGACTGTC-3'
Epha2	5'-GACCTCCCCATCTTCATTTGG-3'	5'-GCGTACAGTGCCCTAGTCATA-3'
Cplx1	5'-GGTGATGAGGAAAAGGACCCC-3'	5'-TCTTGGCGTACTTTGCTTTGC-3'
Chrna5	5'-CTTGAGTACCAACACTGTCCG-3'	5'-CCAGTACTCCAAAGATGCCCT-3'
Chrna2	5'-CATTATCGTCTGCTTCCTGGG-3'	5'-CTTGGAGCCAACATGAGGGA-3'
Chrna7	5'-CTGTAGCTGTCGGTCTTGAGA-3'	5'-CAATGATATGCCGGTGATGGG-3'
Chrnb4	5'-AAACTGATCTGGCTACCTCCC-3'	5'-GTAGAGAGTCCAGGAGATGCC-3'

Alexa Fluor 488 anti-goat	donkey	Thermo Fisher Scientific	A11055	1:1000

Table 2. List of primers used for RT-qPCR

eNeuro Accepted Manuscript

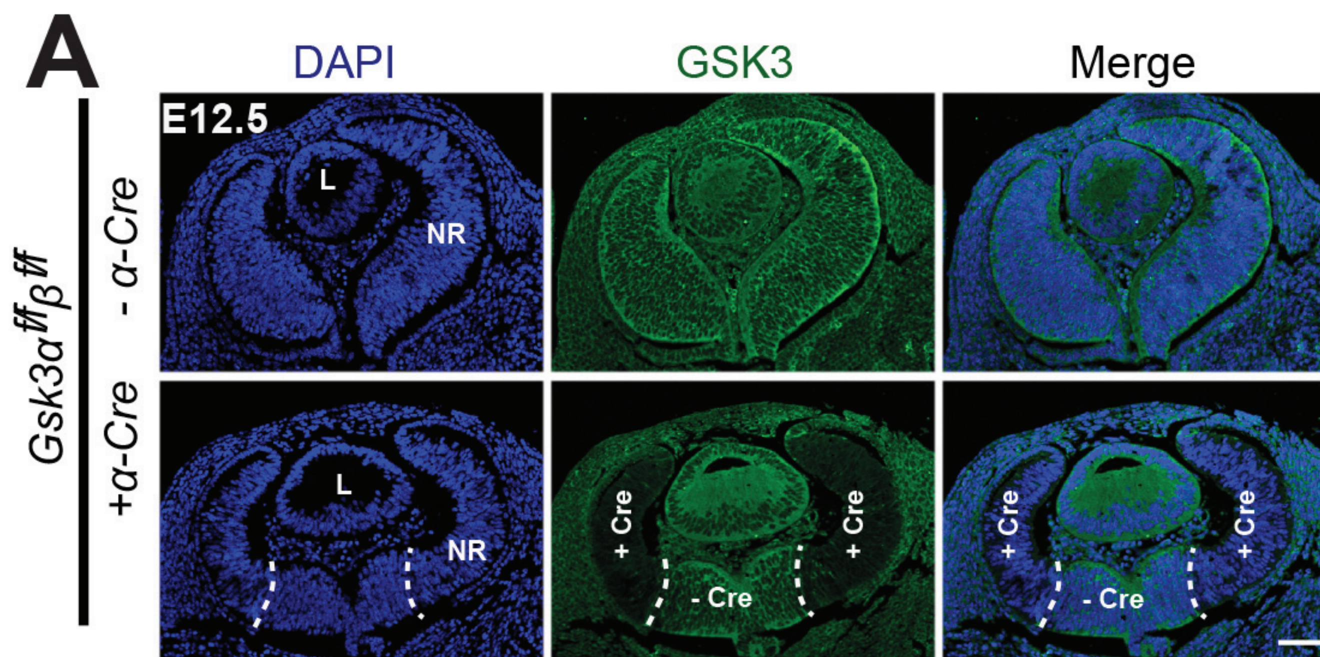

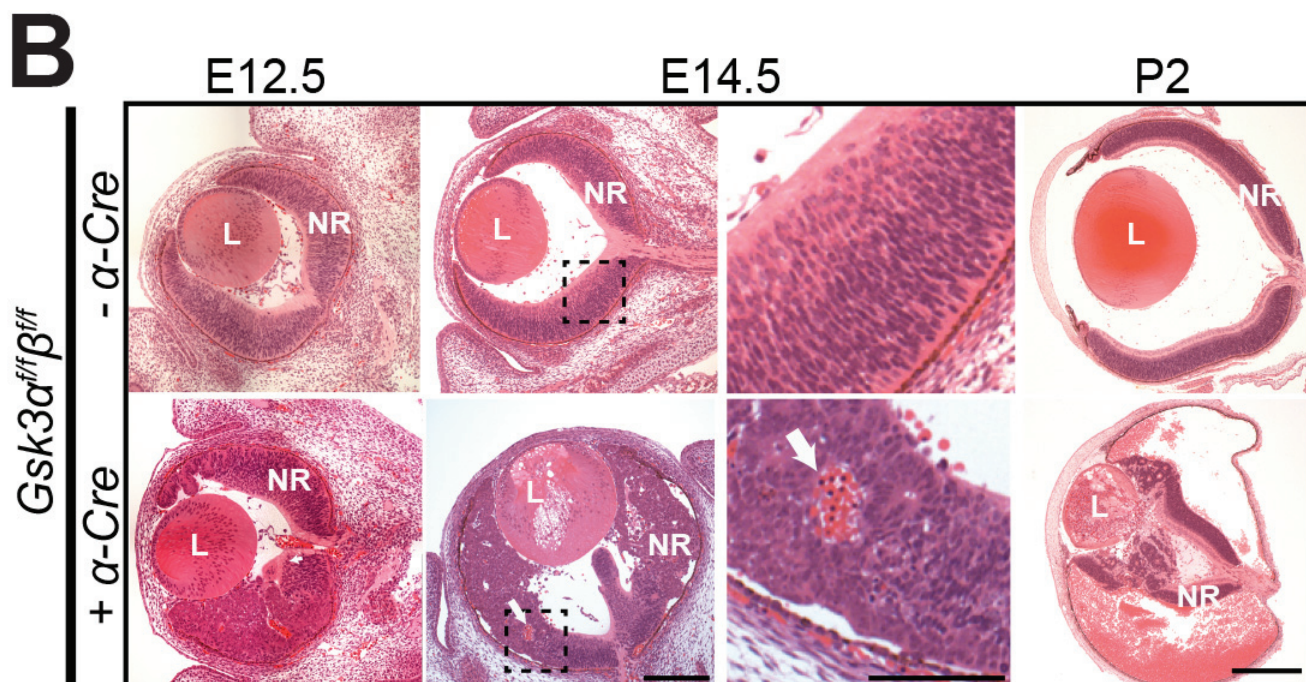

eNeuro Accepted Manuscript

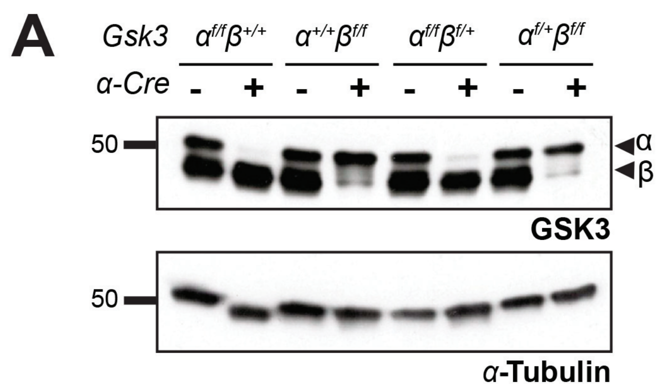

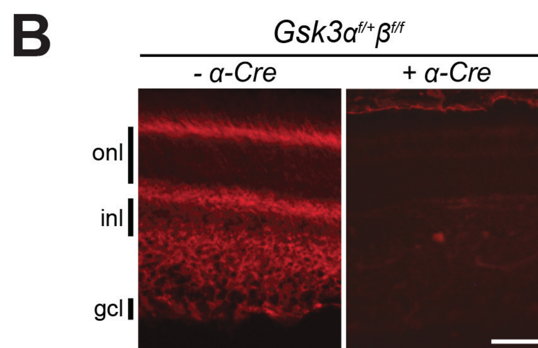

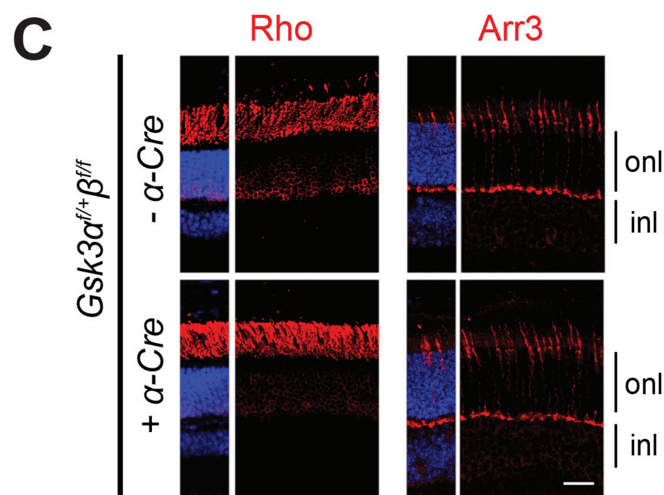

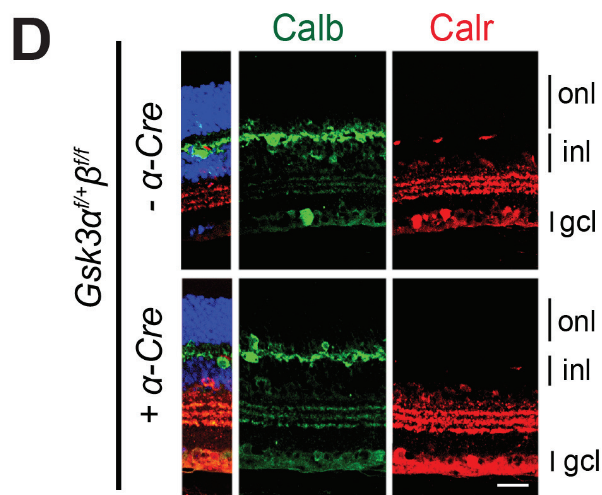

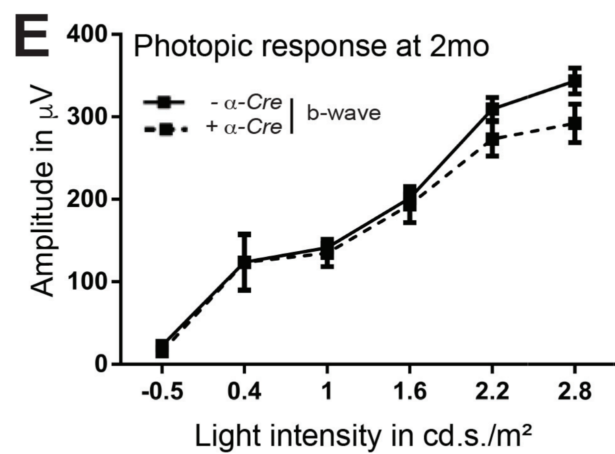

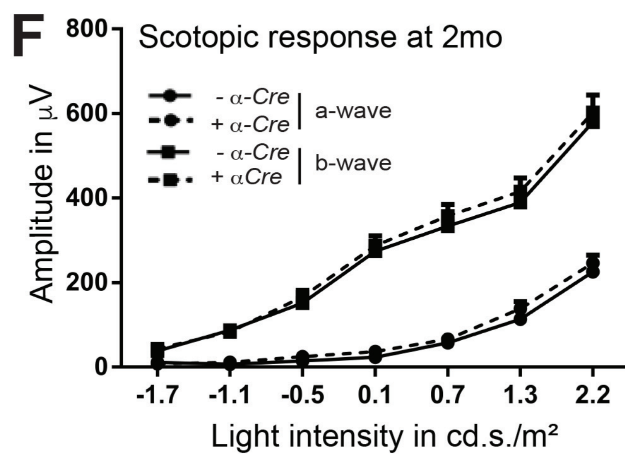

eNeuro Accepted Manuscript

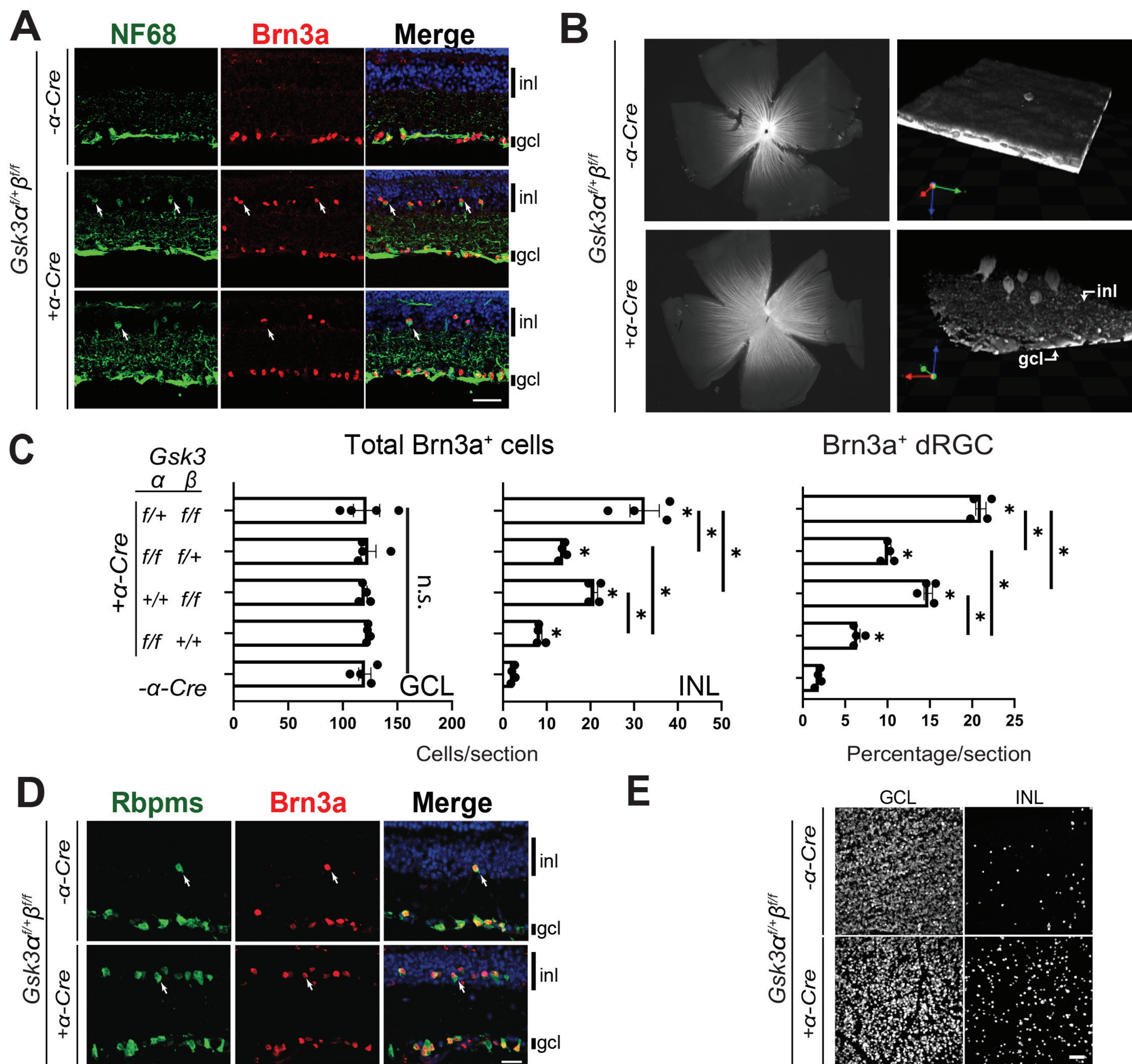

eNeuro Accepted Manuscript

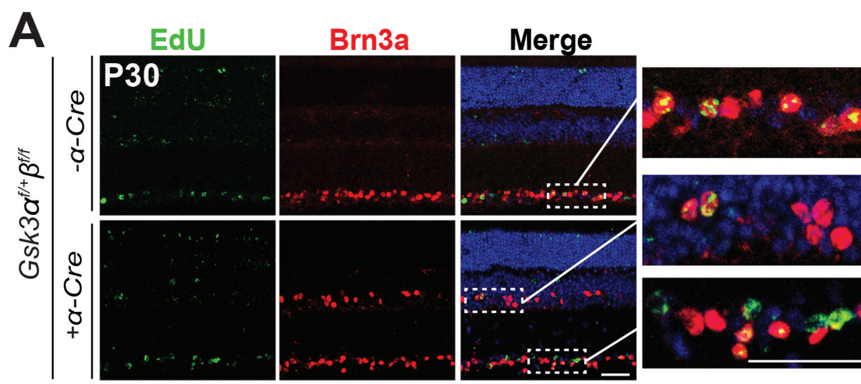

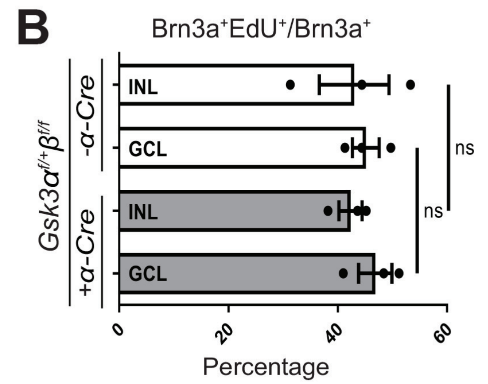

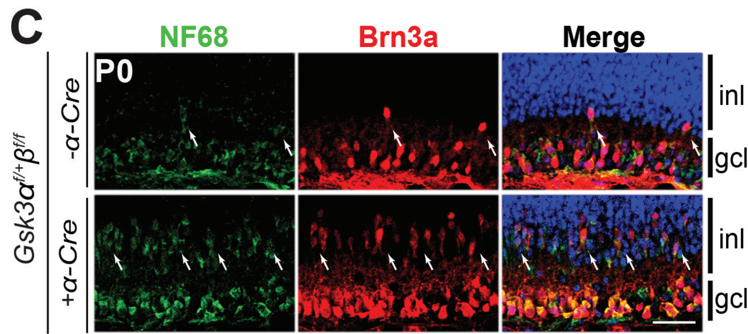

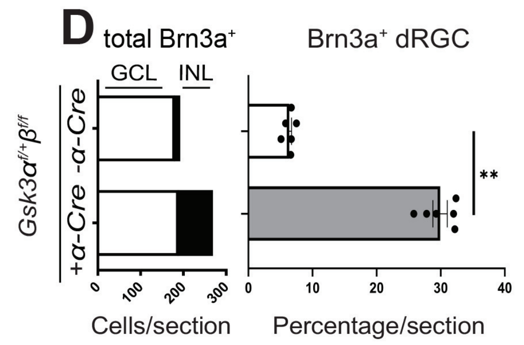

eNeuro Accepted Manuscript

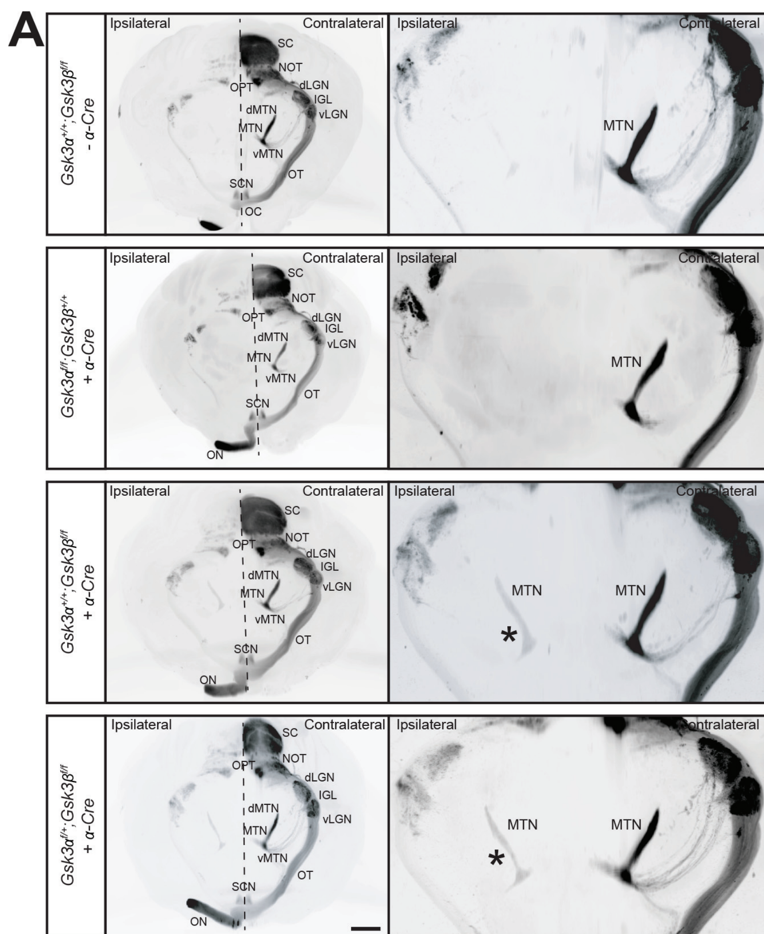

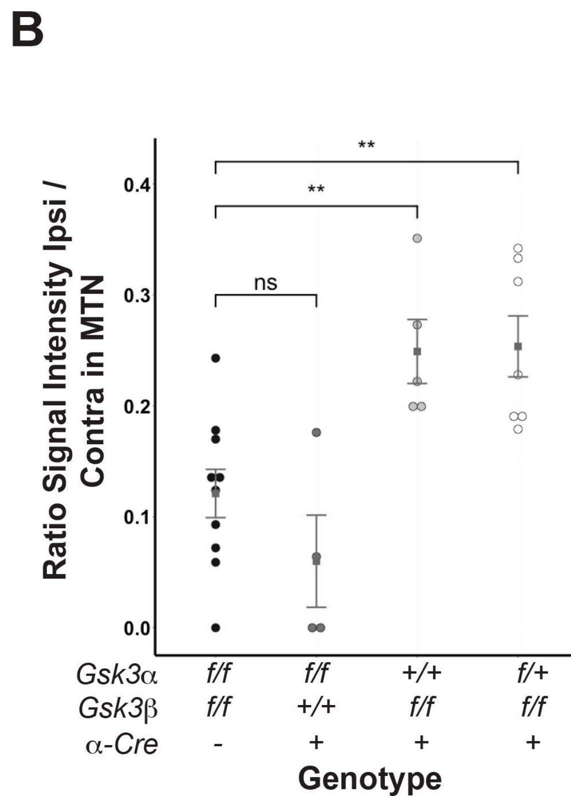

eNeuro Accepted Manuscript